

Article

Comparison of Fluid Flow and Tracer Dispersion in Four-Strand Tundish under Fewer Strand Casting and Sudden Blockage of Strand Conditions

Jintao Song¹, Yanzhao Luo², Yuqian Li¹, Zhijie Guo³, Tianyang Wang¹, Mengjiao Geng¹, Wanming Lin¹, Jinping Fan^{1,*} and Chao Chen^{1,*} 

- ¹ College of Materials Science and Engineering, Taiyuan University of Technology, Taiyuan 030024, China; songjintao0348@link.tyut.edu.cn (J.S.); liyuqian0213@link.tyut.edu.cn (Y.L.); wangtianyang0309@link.tyut.edu.cn (T.W.); 2023510308@link.tyut.edu.cn (M.G.); linwanming@tyut.edu.cn (W.L.)
- ² Shougang Group Co., Ltd., Research Institute of Technology, Beijing 100043, China; luoyanzhao@hotmail.com
- ³ Collaborative Innovation Center of Steel Technology, University of Science and Technology Beijing, Beijing 100083, China; d202210640@xs.ustb.edu.cn
- * Correspondence: fanjinping@tyut.edu.cn (J.F.); chenchao@tyut.edu.cn (C.C.)

Abstract: The study focuses on the four-strand tundish as the research object, aiming at the phenomenon of fewer strand casting (stable blockage) and sudden blockage of the tundish in industrial production. Numerical simulation methods are employed to compare the velocity vectors, flow fields, residence time distribution (RTD) curves, and outflow percentage curves under stable blockage and sudden blockage of the tundishes with a double-weir structure, U-shaped weir structure, and U-shaped weir structure with holes in the front. The results indicate that, after sudden blockage of the tundish strands, the flow field transitions from an unstable four-strand flow field to a stable three-strand flow field. Both the double-weir tundish and the U-shaped weir tundish reach a stable state after 200 s, while the U-shaped weir tundish with holes in the front reaches stability after 150 s. Additionally, compared to other structures, the tundish strands of the U-shaped weir with holes in the front are less affected by blockage, showing better consistency among strands and better adaptability under non-standard casting conditions.



Citation: Song, J.; Luo, Y.; Li, Y.; Guo, Z.; Wang, T.; Geng, M.; Lin, W.; Fan, J.; Chen, C. Comparison of Fluid Flow and Tracer Dispersion in Four-Strand Tundish under Fewer Strand Casting and Sudden Blockage of Strand Conditions. *Metals* **2024**, *14*, 571. <https://doi.org/10.3390/met14050571>

Academic Editors: Henrik Saxen and Noé Cheung

Received: 15 March 2024

Revised: 8 May 2024

Accepted: 10 May 2024

Published: 12 May 2024



Copyright: © 2024 by the authors. Licensee MDPI, Basel, Switzerland. This article is an open access article distributed under the terms and conditions of the Creative Commons Attribution (CC BY) license (<https://creativecommons.org/licenses/by/4.0/>).

Keywords: fewer strand casting; strand blockage; numerical simulation; outflow percentage curve; consistency

1. Introduction

In recent years, tundish metallurgy has emerged as a widely studied field among scholars. To meet the demands of producing clean steel, researchers have employed both physical [1–5] and mathematical [6–11] simulation methods, focusing on the flow of molten steel. This entails optimizing flow control devices [12,13], adjusting process parameters [14,15], implementing gas blowing in the tundish [16,17], and utilizing induction heating technology [18,19]. These endeavors aim to continuously improve the tundish flow field [20,21], temperature distribution [22,23], and enhance inclusion removal efficiency [6,24,25], ultimately elevating the quality of steel products.

Currently, to enhance production efficiency, an increasing number of steel enterprises are turning to multi-strand tundishes. However, this transition has also brought about several adverse effects. In comparison to single-strand or double-strand tundishes, multi-strand tundishes not only feature more complex flow fields but also exhibit significantly increased temperature non-uniformity, making it challenging to maintain consistency between strands. Furthermore, multi-strand tundishes often encounter issues such as strand blockage. The primary cause of strand blockage is operational malfunctions within the tundish, including equipment failures such as mold failure, straightening machines, and electrical faults, as well as process-related problems like steel leakage and blockage in

submerged entry nozzles. Following sudden blockage of a strand in a multi-strand tundish, it is possible for other strands to continue casting.

Researchers have investigated strand blockage in the tundish through physical and numerical simulations, offering detailed descriptions of its impact on tundish flow patterns, temperature distribution, and inclusion removal behavior under abnormal casting conditions [26–37]. Additionally, they have examined the adaptability of various flow control devices. Table 1 provides a summary of the current research status on abnormal casting in tundish strands by scholars.

Table 1. Research Status Status on Abnormal Casting in Tundish Strands.

Investigators	Year	Strand Number	FCD	Mode	Research Focus
C. Bruch, P. Valentin [26]	2004	6	D,W,SR	M	FF
L. Zhang [33]	2005	4	D,WHW	M	FF,HT,IR
L. Zhong et al. [35]	2010	6	WHW	P	FC,FCD
A. Braun et al. [32]	2010	2	SR	P,M	HT
S. K. Mishra et al. [29]	2012	6	/	P,M	FF,HT
A. Sengupta et al. [27]	2013	6	PC	P	FC
W. Xie et al. [30]	2014	7	/	P	FC
J. Zhang et al. [31]	2014	12	WHW	P	FC
T. Merder [28]	2014	6	IP	M	FC
X. Huang [34]	2018	10	/	M	HT,IR
C. Yao et al. [36]	2021	6	WHW	P,M	FCD,HT
J. Fan et al. [37]	2022	4	WHW,SR	P,M	FF,FCD

M—mathematical modeling; P—physical modeling; FCD—flow control device; D—dam; W—weir; SR—stopper rod; WHW—with holes weir; IP—Impact pad; PC—pouring chamber; FF—flow field; HT—heat transfer; IR—inclusion removal; FC—flow characteristic.

In terms of the flow field, C. Buruch and P. Valentin [26] investigated the influence of disturbances, such as the absence of a strand, on the flow behavior in a six-strand tundish through numerical simulation. A water model experiment was conducted by A. Sengupta et al. [27] to investigate strand blockage in a six-strand curved wall of the tundish, and the resulting residence time distribution (RTD) curves were analyzed. In the case of single-strand blockage, from the position nearest to the ladle pouring point to the farthest position from the pouring point, the plug/dead volume (PV/DV) ratio keeps deteriorating at the strands. The severity of the detrimental effect increases with blocking of dual strands in comparison with single-strand blockage. The simulation results of T. Merder [28] showed that, in the case of single-strand blockage, compared with edge strand blockage, after the strand near the ladle shroud was blocked, the ratio of well-mixed volume to dead volume increased, and the ratio of plug volume to dead volume increased, which was similar to the results of A. Sengupta et al. [27] with the water model. S. K. Mishra et al. [29] simulated the velocity vectors at the outlet plane of the six-strand tundish and found that, under normal conditions, a recirculation zone near the outlet promoted a short circuiting trend, and the mixing parameters of the tundish were improved after the near outlet was closed. W. Xie et al. [30] studied the seven-strand tundish, reporting that, after experiencing single-strand and double-strand blockages, both the minimum residence time and average residence time were extended, and the optimal closing schemes for both types of blockages were provided. J. Zhang et al. [31] investigated strand blockage in a 12-strand tundish. Regarding temperature distribution, numerical simulations of the temperature field in a two-strand tundish were conducted by A. Braun et al. [32], revealing that, following single-strand blockage, circulation on the unblocked side is intensified, resulting in colder backflows, which worsen the separation of non-metallic inclusions. Numerical simulation results by L. Zhang [33] indicated that, in a four-strand tundish, the maximum temperature difference during double-strand nozzle blockage is significantly greater than that during single-strand blockage. Similarly, in a study of a ten-strand tundish, X. Huang [34] observed that nozzle blockage leads to an increase in temperature difference within the tundish.

In addition, in terms of flow control devices, L. Zhong et al. [35] studied optimization of the baffle structure, which could extend the residence time and reduce the dead zone volume during non-normal casting operation. The V-shaped baffles in the tundish were improved to U-shaped ones by C. Yao et al. [36], leading to optimization of the tundish flow field after strand closure and a significant improvement in temperature uniformity. The effects of strand blockage in a four-strand tundish under different flow control devices were compared by J. Fan et al. [37]. Through the analysis of outflow percentage, it was found that, after single-strand blockage, the tundish with a U-shaped weir showed better consistency among strands compared to the tundish with a double weir due to its interconnected structure on both sides, and it was noted that the uneven increasing casting speed helped to improve consistency among strands.

Furthermore, the concept of fewer strand casting was initially proposed by C. Yao et al. [36], further studied by X. Wang et al. [38], and was primarily used in multi-strand tundishes. There are two main reasons for this: Firstly, due to the consideration of annual production capacity, costs, and profits by companies, steel production needs to be controlled. In the continuous casting process, this is manifested by the deliberate closure of strands in multi-strand tundishes, resulting in the utilization of an (n-m)-strand tundish instead of an n-strand tundish (where n represents the total number of tundish strands and m represents the number of closed tundish strands). Secondly, fewer strand casting is necessitated by strand blockage in the tundish.

In the research related to fewer strand casting and strand blockage, the different modes of strand blockage (deliberate closure and sudden blockage) have been overlooked by researchers. During numerical simulation calculations, most computations focus solely on steady-state processes, wherein the strands to be closed are set as “wall” to simulate the situation after strand blockage. However, after actual strand blockage, it takes some time for the entire tundish to transition from an n-strand flow field to an (n-m)-strand flow field. This transient process has received little attention in research. Additionally, the aforementioned simulation approach corresponds to the scenario of fewer strand casting in actual production, whereas the simulation process only involves the deliberate closure of tundish strands and does not address the transition process from sudden strand blockage to a stable state.

During water model experiments, differences between sudden blockage and steady state also exist. For example, after completing the flow field test of the n-strand, experimenters close a specific strand, immediately commencing experimental measurements such as residence time distribution (RTD) curves. This process also involves the transition from sudden strand blockage to a stable state. In subsequent experiments, the measurements may reflect the results under steady-state conditions, namely, the outcomes of deliberate closure of fewer strand casting.

J. Fan et al. [37] compared the fluid flow and tracer dispersion of two designs (double weir and U-shaped weir) of tundishes under single-strand blockage and normal conditions. Based on their work, this paper focuses on two casting conditions: fewer strand casting (stable blockage) and sudden blockage. The stable blockage condition is studied and compared with the normal condition in [37]. The sudden blockage condition is studied probably for the first time and reported in the literature. Additionally, a novel weir structure, a U-shaped weir with holes in the front, is studied and compared with the two designs in [37]. Through numerical calculations, this paper simulates the different variations in the flow field after sudden blockage of the tundish strands and the deliberate closure (steady-state fewer strand casting) of the tundish strands for four-strand tundishes with a double weir, U-shaped weir, and U-shaped weir structure with holes at the front. In the sudden blockage scheme, the four-strand open flow fields are calculated. After ensuring that the flow field is stable, the next step of simulating the sudden blockage scheme is performed, that is, adding passive scalars and closing strands at the same time. And a passive scalar is used to track the process of the flow field as it gradually changes from four strands to three strands. In the stable blockage scheme, a certain strand of the tundish is closed,

and then, while calculating the flow field, passive scalars are also added to visualize the evolution of the flow field.

Furthermore, the residence time distribution (RTD) curves and the outflow percentage curves are analyzed to investigate the flow characteristics of the tundishes and the consistency among strands under these two scenarios. This study aims to identify the evolution pattern of the flow field during the transition from sudden strand blockage to steady-state fewer strand casting and to delineate differences in the flow fields, RTD curves, and tracer transport processes between the flow field under complete steady-state fewer strand operation and the flow field after sudden strand blockage, providing theoretical guidance for the flow field and operation of the tundish after sudden strand blockage.

2. Numerical Simulation Methods

2.1. Geometric Dimensions

Based on the geometrical and dynamic similarities principle, a tundish model with a geometrical similarity ratio of 1:3 to an industrial tundish [39] was established. In the industrial tundish, the cross-section of the billet was 150 × 150 mm and the casting speed was 2.3 m/min. Table 2 presents the geometry and operational parameters for the industrial tundish and water model. The dimensions of the tundishes with three different weir structures are illustrated in Figures 1–3.

Table 2. Parameters of the industrial tundish and water model.

Parameters	Volumetric Flow Rate per Nozzle (L/h)	Diameter of the Nozzle (mm)	Depth of Liquid (mm)	Distance between Two Nozzles (mm)	Depth of Shroud Penetration (mm)
Industrial tundish	3105	30	800	1200	220
Water model	199	10	267	400	73

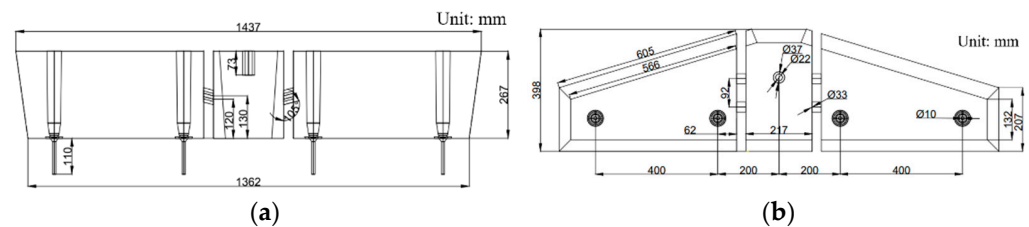


Figure 1. Tundish with double-weir structure: (a) front view, (b) top view. Reprinted from [37].

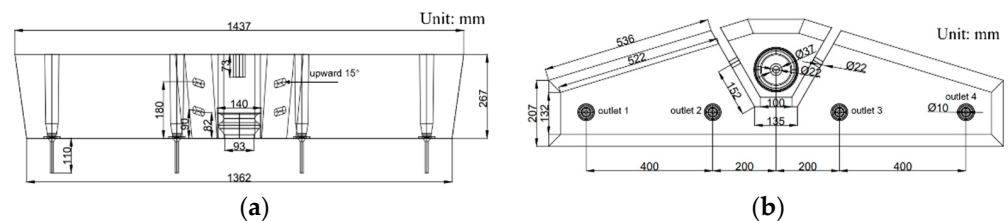


Figure 2. Tundish with U-shaped weir structure: (a) front view, (b) top view. Reprinted from [37].

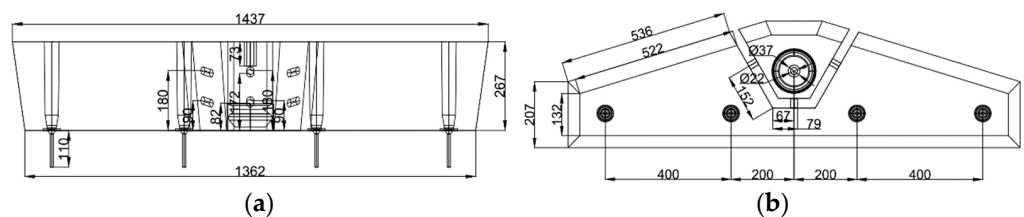


Figure 3. Tundish with U-shaped weir structure with holes in the front: (a) front view, (b) top view.

2.2. Computational Fluid Dynamics (CFD) Modeling and Solution

2.2.1. Model Assumptions

1. Viscosity measurements of liquid iron (steel) [40] and rheology studies [41] performed on liquid steel show non-Newtonian fluid flow characteristics of liquid steel [42]. Water has the same order of magnitude of kinematic viscosity as liquid steel. Physical models, especially water models, are widely used to study the fluid mechanics of liquid steel in industry. For simplicity, the present model was a full-size tundish based on the water model geometry, as shown in Figures 1–3;
2. The realizable k - ε two-layer model [43,44] was used to describe the turbulence phenomenon in the tundish;
3. Passive scalar transport was mainly studied, and it was assumed to be in the liquid phase;
4. For simplicity, thermal buoyancy was neglected and fluid mechanics were the main focus;
5. The free surface was flat, and the slag layer was not considered in the tundish.

2.2.2. Governing Equations

In the CFD (computational fluid dynamics) model, conservation of a general variable ϕ , for example, the density, momentum, enthalpy, or species, within a finite control volume can be expressed as a balance among the various processes, which tend to increase or decrease it. This balance leads to a transport equation with the following general form, according to Patankar [45]:

$$\rho \frac{\partial \phi}{\partial t} + \rho \mathbf{u} \frac{\partial \phi}{\partial x_i} = \frac{\partial}{\partial x_i} \left[\Gamma_{\phi,eff} \frac{\partial \phi}{\partial x_i} \right] + S_{\phi} \quad (1)$$

where ϕ is the variable to be solved, and ρ is the density of the phase, in kg/m^3 . \mathbf{u} is the velocity vector, in m/s . t is the time, in s . x_i is the coordinate. $\Gamma_{\phi,eff}$ is the exchange coefficient, in m^2/s , and S_{ϕ} is the source term given per unit time and volume. The index ϕ represents a specific variable, such as the velocity, turbulent kinetic energy, turbulent dissipation rate, concentration, temperature, etc.

2.2.3. Turbulence Model

The realizable k - ε two-layer model [43], a set of the Reynolds Averaged Navier-Stokes (RANS) turbulence model, was applied to calculate the flow phenomenon in the tundish. This model combines the realizable k - ε model with the two-layer approach (by Rodi [44]). The transport equations for the kinetic energy k and the turbulent dissipation rate ε are given by:

$$\frac{\partial}{\partial t}(\rho k) + \nabla \cdot (\rho k \mathbf{u}) = \nabla \cdot \left[\left(\mu + \frac{\mu_t}{\sigma_k} \right) \nabla k \right] + P_k - \rho \varepsilon \quad (2)$$

$$\frac{\partial}{\partial t}(\rho \varepsilon) + \nabla \cdot (\rho \varepsilon \mathbf{u}) = \nabla \cdot \left[\left(\mu + \frac{\mu_t}{\sigma_{\varepsilon}} \right) \nabla \varepsilon \right] + \frac{\varepsilon}{k} \rho C_{\varepsilon 1} P_k - C_{\varepsilon 2} \rho \frac{\varepsilon^2}{k + \sqrt{\nu \varepsilon}} \quad (3)$$

where

$$P_k = G_k \quad (4)$$

$$P_{\varepsilon} = S_k \quad (5)$$

$$G_k = \mu_t S^2 - \frac{2}{3} \rho k \nabla \cdot \mathbf{u} - \frac{2}{3} \mu_t (\nabla \cdot \mathbf{u})^2 \quad (6)$$

$$S = |\mathbf{S}| = \sqrt{2\mathbf{S} : \mathbf{S}^T} = \sqrt{2\mathbf{S} : \mathbf{S}} \quad (7)$$

$$\mathbf{S} = \frac{1}{2}(\nabla \mathbf{v} + \nabla \mathbf{v}^T) \quad (8)$$

where μ and μ_t are the viscosity of the fluid and turbulent viscosity, respectively, in Pa·s. P_k and P_ε are production terms. G_k is a turbulent production term. S is the modulus of the mean strain rate tensor. σ_k , σ_ε , $\sigma_{\varepsilon 1}$, and $\sigma_{\varepsilon 2}$ are model coefficients and their values are 1, 1.3, 1.44, and 1.92, respectively.

For the two-layer model, the dissipation rate ε near the wall is described as follows:

$$\varepsilon = \frac{k^{3/2}}{l_\varepsilon} \quad (9)$$

where l_ε is a length scale function that is calculated according to Wolfstein [46]:

$$l_\varepsilon = C_l d [1 - \exp(-\frac{Re_d}{2C_l})] \quad (10)$$

$$C_\mu = 0.09 \quad (11)$$

$$C_l = 0.42 C_\mu^{-3/4} \quad (12)$$

where Re_d is the wall distance Reynolds number. d is the distance to the wall, in m. C_l is the model coefficient.

2.2.4. Tracer Transport

The passive scalar transport model was used to predict the transport process of the tracer in the water, and the model can be described as follows:

$$\frac{\partial}{\partial t}(\rho\omega) + \nabla \cdot (\rho\mathbf{u}\omega) = \nabla \cdot (\rho D_{eff} \nabla \omega) \quad (13)$$

where ω is the volume fraction of the scalar tracer in the computational domain. D_{eff} is the effective diffusion coefficient of the passive scalar, in m^2/s . ω , the outlet cross-sectional area averaged, was used as the outlet value for the analysis of the RTD curve. A similar set of scalar tracers was used in [47,48].

2.2.5. Mesh

The 3D geometric models of the tundishes were established. A polyhedral mesh was used in the simulation, as shown in Figures 4–6.

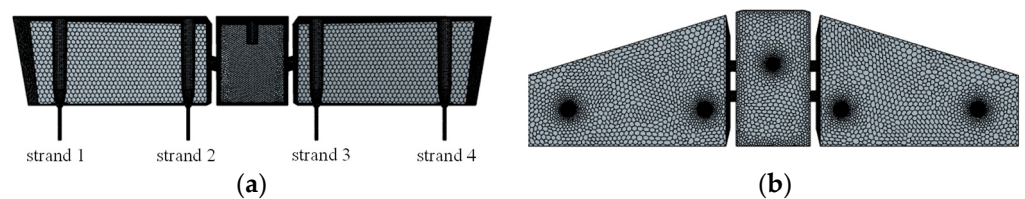


Figure 4. Mesh of double-weir four-strand tundish: (a) front view, (b) top view.

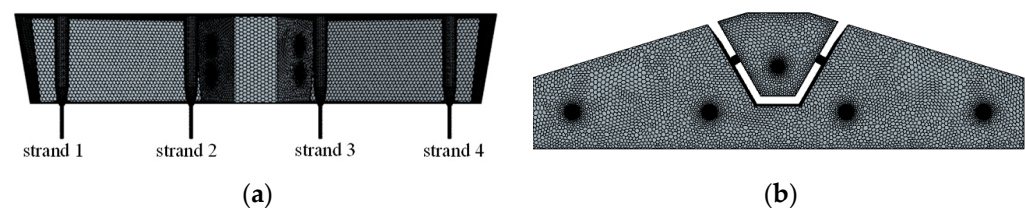


Figure 5. Mesh of U-shaped weir four-strand tundish: (a) front view, (b) top view.

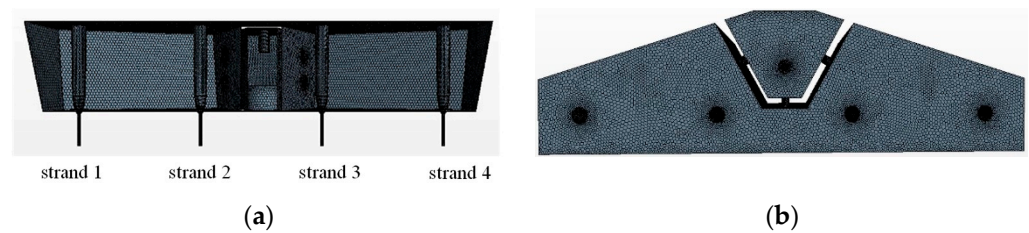


Figure 6. Mesh of U-shaped weir four-strand tundish with holes in the front: (a) front view, (b) top view [37].

2.2.6. Boundary Conditions

1. No-slip conditions were applied at all solid surfaces for the liquid phase;
2. A constant inlet velocity was used, and the inlet velocity was 0.58 m/s;
3. At the tundish outlet, an outflow boundary with a constant mass flow rate condition was applied;
4. The outlet pressure was set to a constant value of one standard atmosphere;
5. The roughness of the turbulence inhibitor, inlet ladle shroud, and stopper rod was set as 1×10^{-5} m. In addition, the roughness of other solid walls was set as 2×10^{-6} m.

2.2.7. Treatment of Sudden Blockage and Fewer Strand Simulation

In the sudden blockage scheme, a convergent flow field steady simulation of all four-strand open tundishes was used as the basic case for the transient simulation. When the transient simulation started, one or two strands were closed by setting the outlet as wall, and the tundish changed from four strands to three strands. The flow field and streamline changed until a stable fewer strand flow field was formed. To track the complex flow field evolution, the tracer (passive scalar) was injected into the inlet of the tundish when the transient simulation started. By contrast, the transient simulation of the fewer strand scheme was based on the convergent flow field steady simulation with one or two strands closed. When the transient simulation started, the tundish maintained a stable flow field and the tracer was injected into the inlet. The evolution of the tracer was used to track the flow field, like many research papers have done.

In this study, the pulse injection time interval was 0.226, in order to guarantee the identical volume of tracer in the water model (50 mL). The injection time was calculated from the volume of tracer added in the water model experiment and the inlet cross-sectional area and the inlet velocity of the tracer in the numerical simulation. In the simulation, $\omega = 0$ in the whole region cells, except the tracer injection cells, while in the tracer injection cells, $\omega = 1$.

2.2.8. Solution Procedure

The governing equations were solved by using finite volume method-based software Simcenter Star-CCM+ (17.02.007-R8) [49]. The steady-state simulation was iteratively calculated by the turbulence model. As described before, the initialization of the transient simulation of the sudden blockage scheme started from the steady simulation of the four strands open case. The initialization of the transient simulation of the fewer strand scheme started from the steady simulation of the corresponding three strands open case. The solution algorithms for velocity and pressure were calculated using the SIMPLE method. The convergence criterion was that the residual values of all variables were less than 1×10^{-3} . For the transient simulation, the time step was gradually increased, the initial time step was 0.002 s and the maximum time step was 0.5 s, and each time step included 30 iterations.

2.3. Analytical Method

2.3.1. RTD Analysis Method

The concentration–time variation curves of the tracer in the numerical simulation process were obtained using the stimulus–response method. The monitoring points for the RTD curves were all located at the tundish outlet. The RTD curve can be obtained according to the following formula:

$$E(\theta) = C(\theta) / \int_0^{\infty} C(\theta) d\theta \quad (14)$$

$$\theta = \frac{t}{t_{\text{theory}}} \quad (15)$$

$$t_{\text{theory}} = \frac{V}{Q_{\text{in}}} \quad (16)$$

$$E(\theta) = \frac{C(\theta)}{\sum_{\theta=0}^{\theta_{\text{max}}} C(\theta) \Delta\theta} \quad (17)$$

where $E(\theta)$ is the dimensionless concentration of the outlet at dimensionless time θ . $C(\theta)$ is the volume fraction ω of the outlet at dimensionless time θ . θ_{max} is the maximum monitoring time in dimensionless form. t is the monitoring time. t_{theory} is the theoretical residence time. V is the volume of liquid in the tundish. Q_{in} is the volume flow rate at the tundish inlet.

2.3.2. Outflow Percentage Analysis Method

This study adopted the outflow percentage analysis method proposed in the previous publication by Fan et al. [37]. The percentage of outflow refers to the ratio $w_i(t)$ of the mass of the tracer flowing out of the outlet at the time interval from t to $t + \Delta t$ to the total mass of the tracer added in the inlet. In addition, the cumulative tracer outflow percentage $W_i(t)$ could be obtained by an integral of $w_i(t)$ with time from 0 to t . This method can avoid distortion of the data during dimensionless normalization. The formula for calculating the outflow percentage is as follows:

$$w_i(t) = m_i(t) / M \quad (18)$$

$$M = \rho_{\text{tracer}} Q_{\text{in}} \omega_0 \Delta t' \quad (19)$$

$$m_i(t) = \rho_{\text{tracer}} Q_{\text{out},i} \omega_i(t) \Delta t \quad (20)$$

$$W_i(t) = \sum_{t=0}^t w_i(t) \quad (21)$$

where $m_i(t)$ is the mass of the tracer flowing out of strand i of the four-strand tundish at the time interval from t to $t + \Delta t$, in kg. M is the total mass of the tracer added in the inlet, in kg. ρ_{tracer} is the density of the added tracer, in kg / m³. ω_0 is the volume fraction of the input tracer. $\Delta t'$ is the time interval of the injection tracer, in s. $Q_{\text{out},i}$ is the volume flow rate at the outlet of strand i in the multi-strand tundish, in L/s. $\omega_i(t)$ is the volume fraction of the tracer flowing out of strand i of the four-strand tundish at the time interval from t to $t + \Delta t$. In the numerical simulation, $\omega_i(t)$ is calculated by monitoring the ω value of each strand of the tundish multiplied by the time step interval Δt .

3. Results and Discussion

3.1. Mesh Sensitivity and Validation

As depicted in Figure 7, mesh independence validation was conducted for the tundish model with mesh numbers of 338,809, 635,071, and 962,897, respectively. The simulation results were also compared with the experimental results. The RTD curves for strand 1 remain consistent with the three mesh sizes, while for strand 2, the consistency is poorer with coarser mesh, but better with the other two mesh sizes. Additionally, the gray shaded part in Figure 7 represents the fluctuation range of the physical model experimental data, and the results of mesh 2 show good agreement with the experiment results. Considering accuracy and computational load, this study adopted a mesh number of 635,071 (mesh 2).

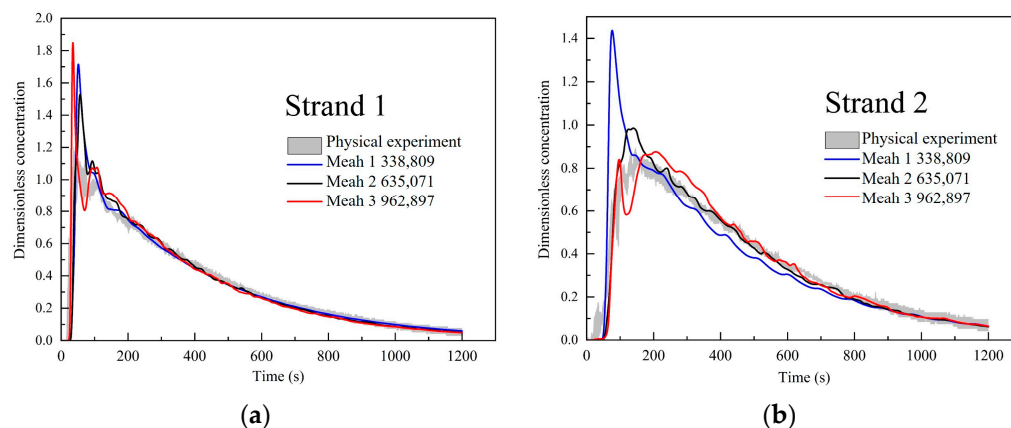


Figure 7. RTD curve verification for different mesh numbers: (a) strand 1; (b) strand 2.

3.2. Velocity Distributions of Tundishes with Three Weir Structures under Normal Conditions

Figures 8–10 depict the velocity vector distributions of the tundishes with a double weir, U-shaped weir, and U-shaped weir with holes at the front under normal casting conditions. In the case of the tundish with a double weir, the mainstream area is observed to form a basic symmetric circulation pattern from the front view. When observed from the top perspective, the stream is flow-directed into the tundish area by two sets of guide holes. One stream flows along the inclined wall surface, passing through the side wall, and forms a circulating flow around the outside stopper rod. Another stream forms a circulation near the inner stopper rod, as illustrated in Figure 8.

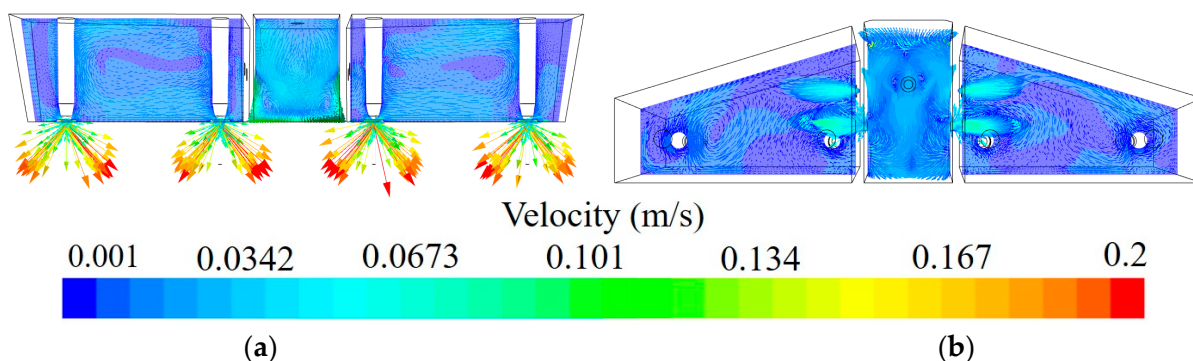


Figure 8. Velocity vector diagram of double-weir tundish under normal conditions: (a) front view; (b) top view.

In the tundish with a U-shaped weir, from the front view, the flow is guided by the guide holes to flow diagonally upward along the free surface in the mainstream area, forming a circulating flow around the outside stopper rod and the bottom of the tundish.

Particularly, at the connection point of the front part of the U-shaped weir, the left and right flows converge, forming a symmetrical circulating flow, as shown in Figure 9.

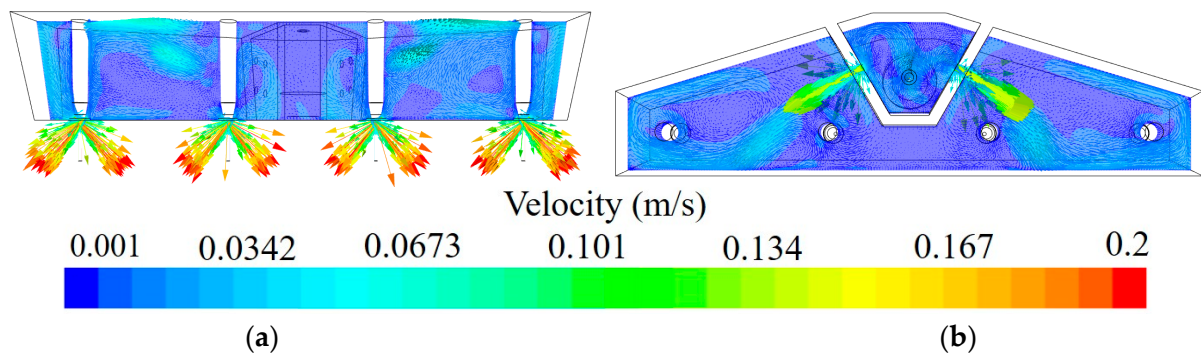


Figure 9. Velocity vector diagram of U-shaped weir tundish under normal conditions: (a) front view; (b) top view.

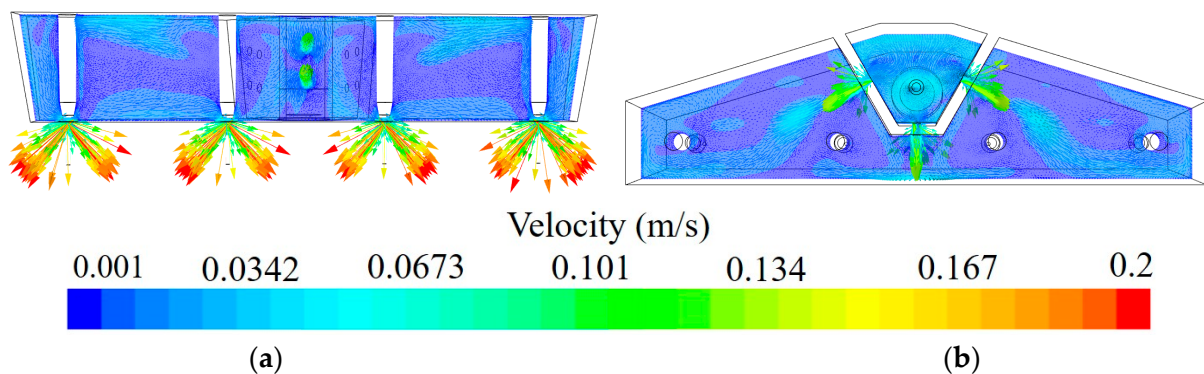


Figure 10. Velocity vector diagram of U-shaped weir structure with holes at the front under normal conditions: (a) front view; (b) top view.

For the U-shaped weir structure with holes at the front, regardless of the front or top view, the flows form a symmetrical circulating pattern. Particularly, due to the presence of guide holes at the front of the weir, the flows replenish to the sides after passing through the front wall of the tundish. From the top view, compared to the other two structures, the circulation near the inner stopper rod is weakened, as shown in Figure 10.

3.3. Transport Process of the Tracer under Different Blocking Conditions in the Tundish with a Double Weir

Figure 11 depicts the velocity vector diagram of the tundish with a double weir shortly after sudden blockage of strand 1 and shortly after it became stable. The red dashed boxes in Figure 11 are the middle and upper part of stopper rod 1 respectively. Under the sudden blockage scheme, on the blocked side, the mainstream passes through the middle region of stopper rod 1 in a counterclockwise direction along the free surface, reaches the bottom of the tundish, and flows through strand 2 along the bottom, ultimately forming a smaller counterclockwise circulation in the mainstream area. Under the stable blockage scheme, the flow on the blocked side passes along the free surface in a counterclockwise direction, reaches the bottom of the tundish through the upper part of stopper rod 1, flows out through strand 2 along the bottom, and ultimately forms a larger counterclockwise circulation in the mainstream area. Overall, the difference in velocity distribution in the mainstream area of the unblocked side of the double-weir tundish is small, but under the same scheme, there is a significant difference in velocity distribution between the left and right sides. Figure 12 shows the velocity vector distribution of the tundish shortly after sudden blockage of strand 1 at 1200 s. It is evident from the figure that under the sudden

blockage scheme, after the flow field stabilizes, the velocity vector distribution is essentially consistent with that shortly after the stable blockage scheme.

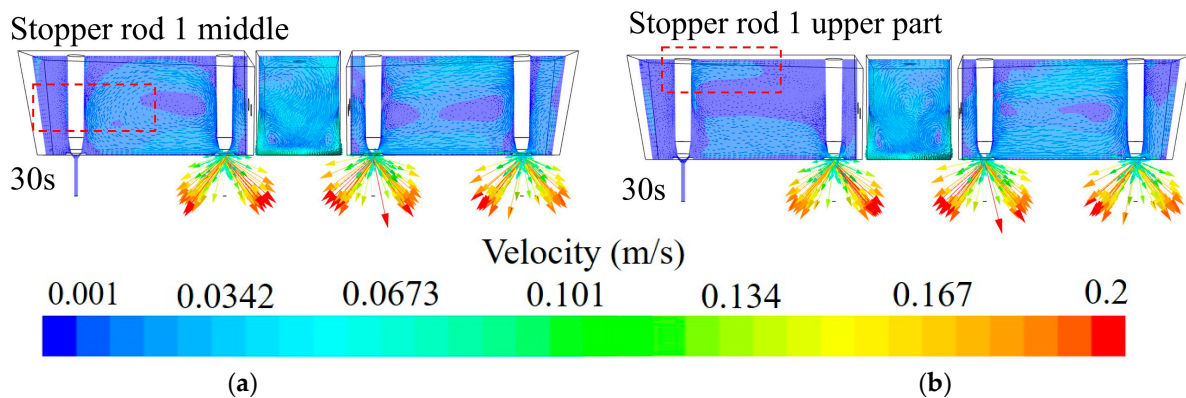


Figure 11. Velocity vector diagram of double-weir tundish after strand 1 blockage at 30 s: (a) sudden blockage; (b) stable blockage.

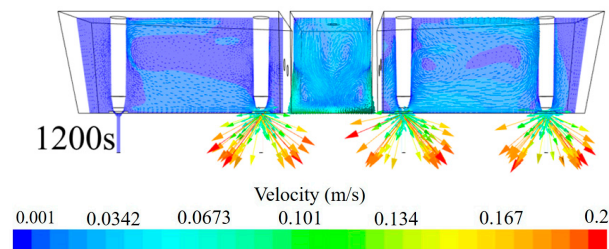


Figure 12. Velocity vector diagram of tundish at 1200 s after sudden blockage of strand 1.

Figure 13 illustrates the streamline variations resulting from blockage of strand 1 in the tundish with a double weir. Figure 13a illustrates the sudden blockage scenario, while Figure 13b illustrates the stable blockage scenario. After blockage of strand 1, the tracer was introduced into the pouring chamber from the ladle shroud, and the movement states of both scenarios within the pouring chamber are essentially identical, as depicted in the schematic diagram in Figure 14. In the sudden blockage scenario, the mainstream area on the blocked side experiences initial period dynamism; the original flow field undergoes continual changes. Following the flow of fluid from the guide holes to the left mainstream area, a small amount of the tracer is observed to exhibit clockwise motion around stopper rod 1 from a top-down perspective, while a significant amount of the tracer is transported counterclockwise along the right side of stopper rod 1 to reach the bottom of the tundish, and then flows counterclockwise into strand 2 along the bottom of the tundish. Subsequently, the tracer gradually homogenized within the left region of the tundish, a process closely resembling that under normal operating conditions. Around 200 s, a stable counterclockwise circulation gradually emerges. The flow trends within the unblocked side of the mainstream area are similar to that under normal operating conditions. At 230 s, the tracer concentration in the mainstream area on the right side is markedly higher than that on the left side.

Under the stable blockage condition, the tracer flowing out from the guide holes is not, as under the sudden blockage condition, primarily carried by the flow field along the right side of stopper rod 1 in a counterclockwise direction to reach the bottom of the tundish and then gradually dispersed toward the left side of stopper rod 1. Instead, it is carried along the free surface to reach the left side of stopper rod 1, following the stable counterclockwise circulation flow field (from a frontal perspective) as it flows toward each strand. Thus, the initial flow field under the stable blockage condition is essentially consistent with the stable flow field formed around 200 s after sudden blockage. After approximately 200 s of fluctuation in the tundish flow field under the sudden blockage condition, the flow

field transitions from a constantly changing state to a stable state, ultimately reaching the initial flow field of the stable blockage condition. At 230 s, the tracer concentration in the mainstream area on the right is also significantly higher than that on the left. Compared to the sudden blockage condition, the concentration difference between the two sides in the stable blockage condition is noticeably reduced.

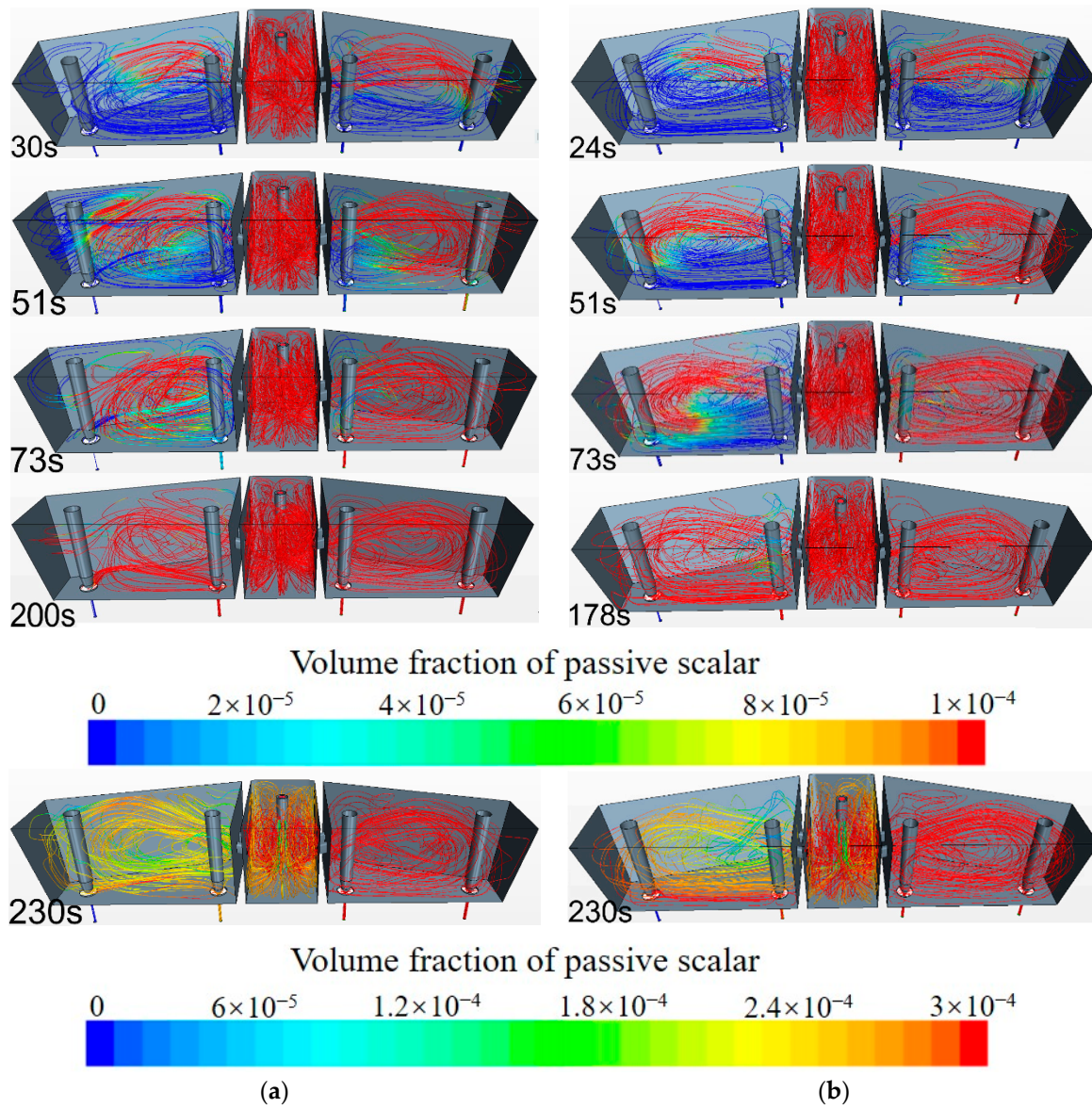


Figure 13. Streamline diagram of the double-weir tundish with strand 1 blocked: (a) sudden blockage, (b) stable blockage.

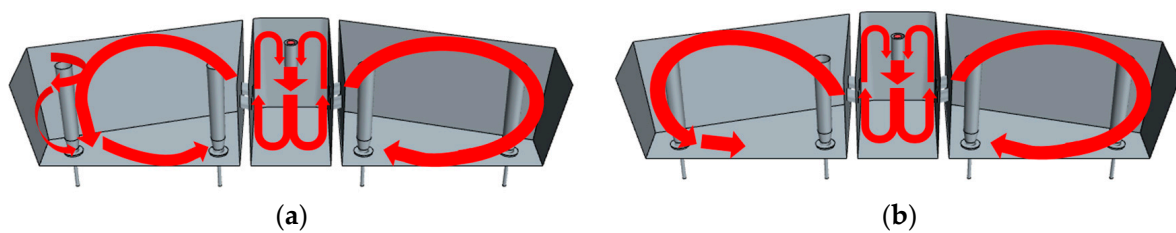


Figure 14. Flow field diagram of the double-weir tundish with strand 1 blocked at 73 s: (a) sudden blockage, (b) stable blockage.

Figure 15 depicts the velocity vector diagram of the tundish with a double weir shortly after sudden blockage of strand 2 and shortly after it becomes stable. The red dashed boxes in Figure 15b represents the area of significant difference in vector field. Under the sudden blockage scheme, the stream flows are directed counterclockwise along the free surface in the mainstream area, flowing out from strand 1, while most of stream forms a circulating flow along the bottom of the tundish. Under the stable blockage scheme, the flow reaches strand 1 along the free surface via the left side wall of the tundish, with only a small portion of the stream directed toward strand 2 along the bottom of the tundish. Figure 16 depicts the velocity vector diagram of strand 2 in the double-weir tundish at 1200 s after sudden blockage. The red dashed boxes in Figure 16 indicate the major velocity vector distribution areas. The main velocity distribution includes flow along the free surface, flow along the side wall, and a small portion of flow along the bottom, which is essentially consistent with the velocity vector distribution shortly after stable blockage.

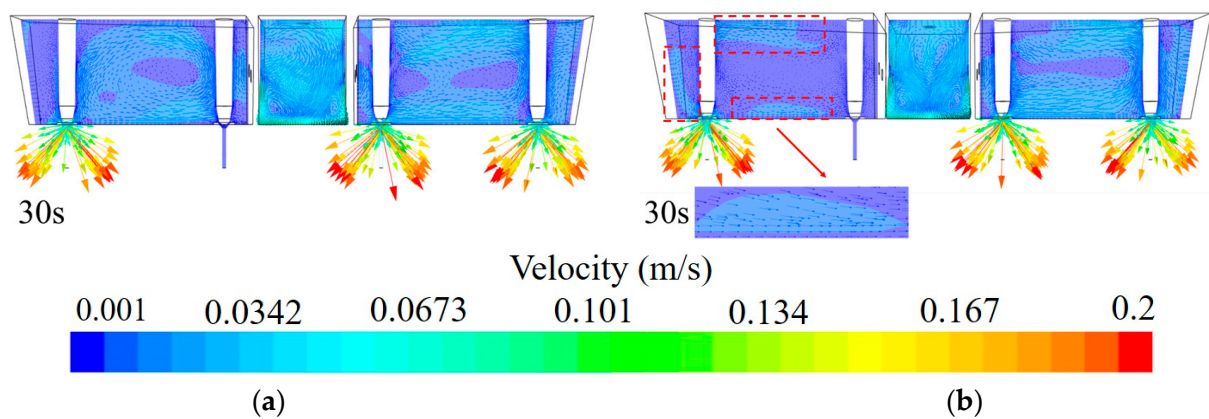


Figure 15. Velocity vector diagram of double-weir tundish after strand 2 blockage at 30 s: (a) sudden blockage; (b) stable blockage.

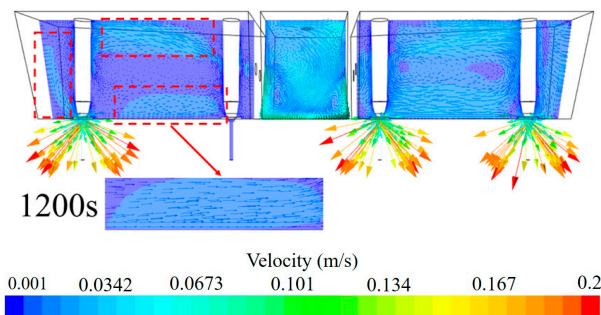


Figure 16. Velocity vector diagram of tundish at 1200 s after sudden blockage of strand 2.

Figure 17 depicts the streamline variations caused by blockage of strand 2 in the tundish with a double weir. After blockage of strand 2, the tracer was introduced into the pouring chamber from the ladle shroud, and the movement states of both scenarios within the pouring chamber are essentially consistent. Under the sudden blockage condition, the mainstream area on the blocked side also undergoes dynamic changes. Unlike the situation where strand 1 is blocked, where some fluid flows directly to strand 1 in a “short-circuit flow” manner after flowing from the guide holes to the vicinity of stopper rod 1, as shown in Figure 18, the remaining fluid flows counterclockwise along the bottom of the tundish to reach strand 2. Around 200 s, a stable counterclockwise circulation flow (from a frontal perspective) gradually forms, and the disturbance in the flow field dissipates almost completely after 200 s. The flow field transitions to a stable state and tends to stabilize. The flow trend on the unblocked side of the mainstream area is similar to that under normal operating conditions. At 230 s, the tracer concentration in the mainstream area on the

the bottom of the tundish to reach strand 2. The counterclockwise circulation formed, compared to blockage of strand 1, is more biased toward the left side of stopper rod 1. By 230 s, the concentration of the tracer in the main flow area on the right side is significantly higher than that on the left side, and the concentration difference between the two sides is significantly higher than when strand 1 is blocked and slightly lower than the situation of sudden blockage.

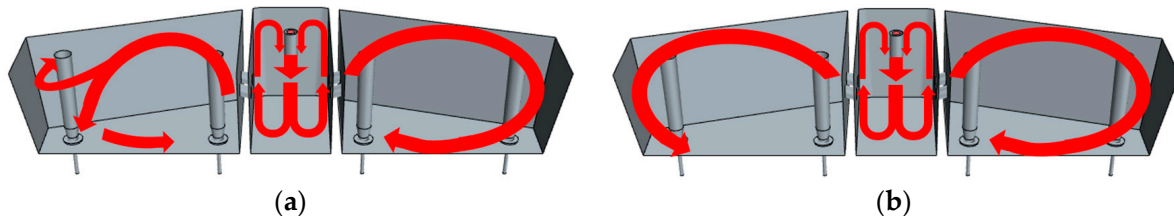


Figure 18. Flow field diagram of the double–weir tundish with strand 2 blocked at 73 s: (a) sudden blockage, (b) stable blockage.

3.4. Transport Process of the Tracer under Different Blocking Conditions in the Tundish with a U-Shaped Weir

Figure 19 depicts the velocity vector diagram of the U-shaped weir tundish shortly after sudden blockage of strand 1 and stable blockage. The red dashed boxes in Figure 19a represent the main difference area of the velocity vector field. Overall, the velocity field shows the stream flow passing along the free surface, through the side walls of the tundish, reaching the outer strand, and finally transported along the bottom of the tundish toward the inner strand. The unblocked side of the tundish is also affected due to the connection between the left and right sides of the tundish; especially under the sudden blockage scheme, the right intermediate area is influenced by the inflow from the front side of the U-shaped weir, where two streams converge to form an upward flow, as shown in Figure 19b. There is a noticeable difference in the velocity vector distribution between the sudden and stable blockage schemes. Figure 20 shows the velocity vector results of the tundish at 1200 s after sudden blockage of strand 1. On the blocked side, the stream flows out from strand 2 in a stable counterclockwise circulation, while on the unblocked side, the upward flow disappears and develops into a flow stream along the bottom from strand 4 to strand 3.

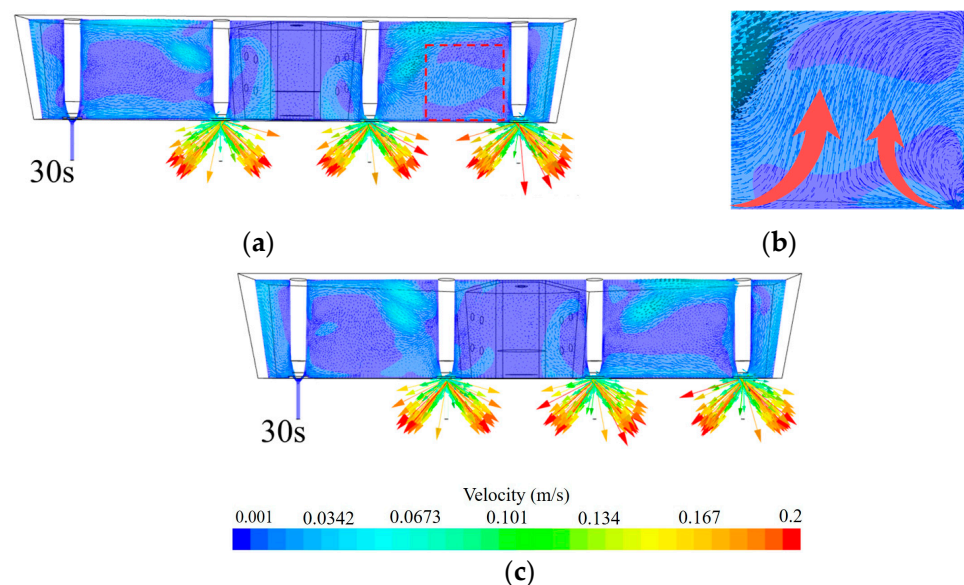


Figure 19. Velocity vector diagram of U-shaped weir after strand 1 blockage at 30 s: (a) sudden blockage; (b) partial magnification; (c) stable blockage.

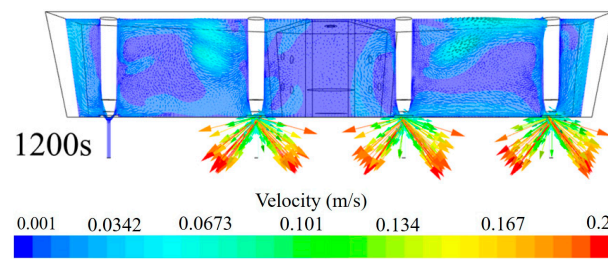


Figure 20. Velocity vector diagram of the tundish at 1200 s when strand 1 is suddenly blocked.

Figure 21 shows the streamline variation diagram under single-strand blockage in the tundish with a U-shaped weir. After blockage of strand 1, the tracer was introduced into the pouring chamber from the ladle shroud, and the movements in the pouring chamber under both schemes are essentially consistent. In the example of the left mainstream area, under the sudden blockage scheme, the fluid flows straight toward stopper rod 1 after being discharged from the diversion holes of the U-shaped weir, with some fluid forming clockwise (viewed from above) recirculation in the upper part of the tundish, and another part flowing to strand 1 in a “short-circuit flow” manner. The main flows in the middle and lower portions of the tundish are directed counterclockwise (viewed from the front) along the inclined wall toward the mainstream area, and then were uniformly mixed throughout the entire tundish, resulting in a flow field that is essentially consistent with that under normal operating conditions. Additionally, due to the absence of isolation on both sides of the tundish, it can be observed that flows pass from the left side through the front of the U-shaped weir to reach strand 3 on the right side. Figure 22 depicts the velocity vector distribution of the U-shaped weir tundish at 1200 s after sudden blockage of strand 1. From the top view, the flow streams on the left and right sides of the tundish exhibit a symmetric distribution, with the velocity field slightly stronger on the blocked side than on the unblocked side. Upon closer inspection in the zoomed-in section, the flow streams from the front side of the U-shaped weir distribute from right to left.

As for the concentration of the tracer on both sides, since outlet 1 is closed, the total amount of the tracer flowing out from the left side is less than that from strands 3 and 4 on the right side. Therefore, the concentration of the tracer on the left side of the tundish is significantly higher than that on the right side, and this situation persists after 250 s, as shown in the figure. As the mainstream areas on both sides are connected, the high-concentration tracer on the left side mixes with the right side through the front of the U-shaped weir until it is uniformly mixed throughout the entire tundish, as shown in Figure 23.

Under the stable blocking scheme, in the example of the left mainstream area, the tracer is discharged from the diversion holes of the U-shaped weir and reaches the left side of stopper rod 1 along the free surface, and then arrives at strand 1 counterclockwise (viewed from the front) along the left side of stopper rod 1. The tracer reaches strand 2 along the bottom of the mainstream area and is mixed uniformly within this area. The transport process of the tracer on the right side remains essentially symmetrical to that on the left side. After mixing on both sides, due to the absence of isolation on both sides of the tundish, it can be observed that tracer from the left mainstream area further mixes with the right side through the front of the U-shaped weir. Consistent with the sudden blockage scheme, under the stable blocking scheme, the concentration of the tracer on the left side of the tundish is significantly higher than that on the right side, and the concentration difference is essentially consistent with that under sudden blockage.

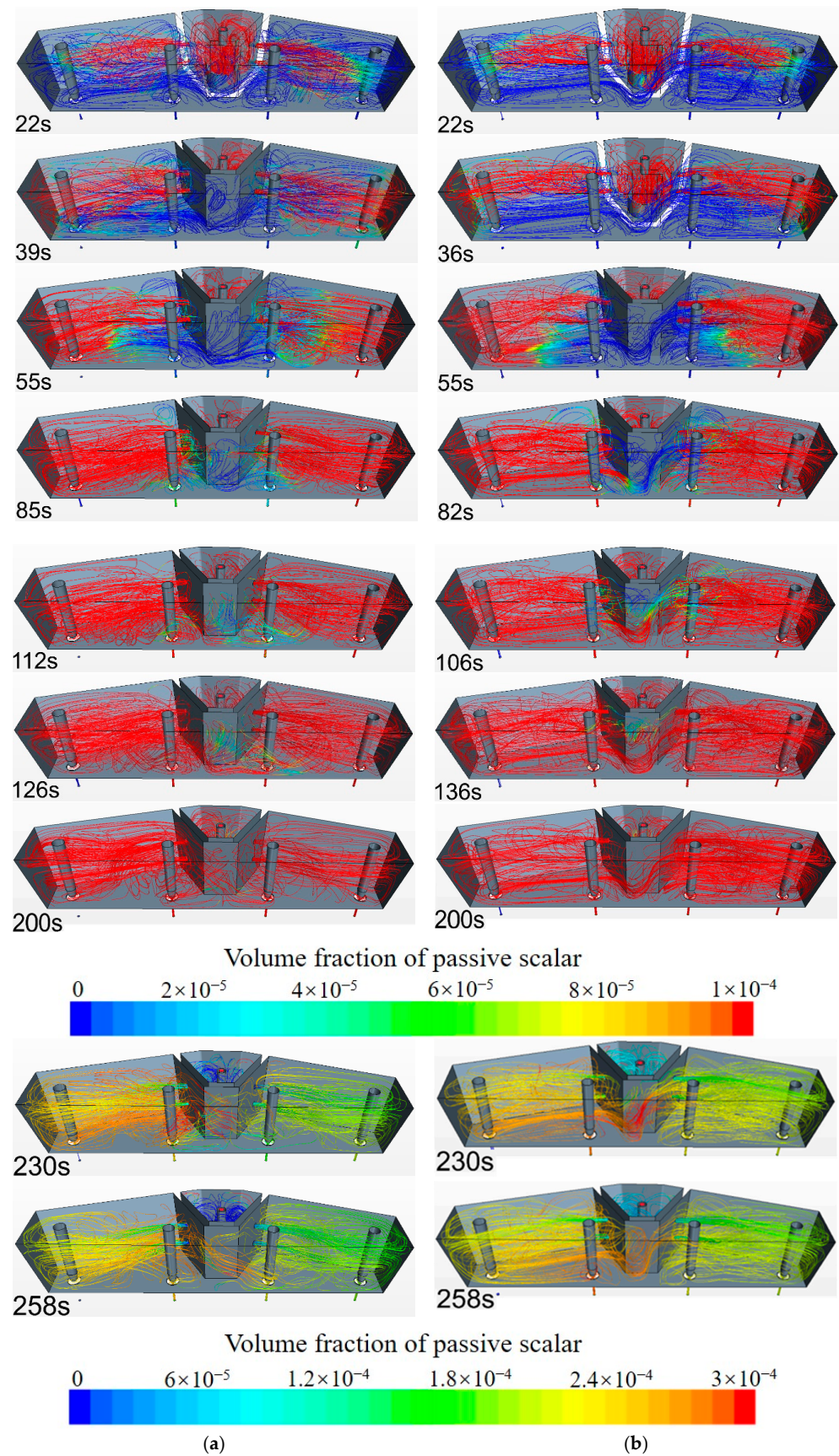


Figure 21. Streamline diagram of the U-shaped weir tundish under strand 1 blockage: (a) sudden blockage, (b) stable blockage.

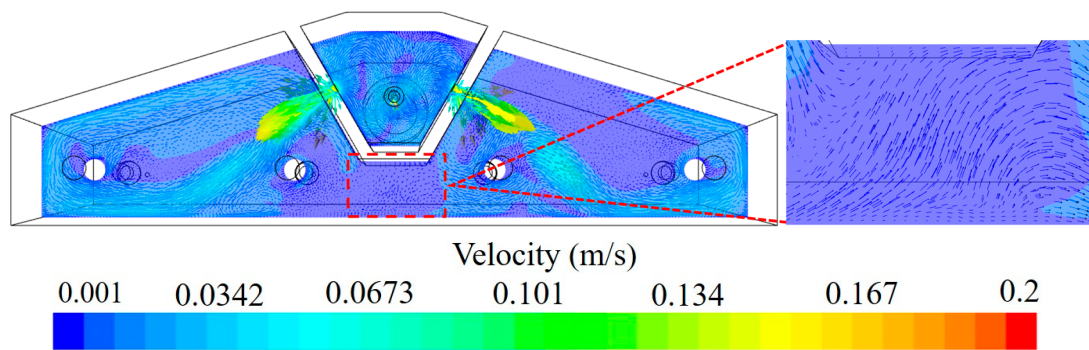


Figure 22. Velocity vector distribution of U-shaped weir tundish after strand 1 sudden blockage at 1200 s.

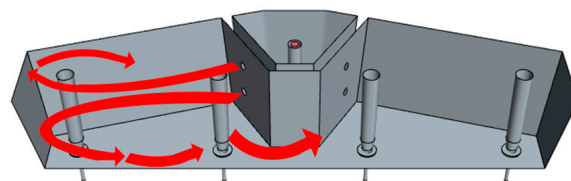


Figure 23. Flow field diagram of the U-shaped weir tundish under strand 1 blockage.

Figure 24 depicts the velocity vector distribution of the U-shaped weir tundish at 1200 s after strand 2 sudden blockage. Compared to blockage of strand 1, the circulation on the blocked side is slightly weakened, while the velocity field at strand 2 is enhanced. The streams flow from the front side of the U-shaped weir from left to right. Overall, the flow field is essentially consistent with that after blockage of strand 1. Following mixing on both sides, the concentration of the tracer on the left side is slightly higher than that on the right side, and the concentration difference between the two sides is significantly lower than that after blockage of strand 1. This is because after blockage of strand 2, the flow stream exits earlier from strand 1, resulting in a lower accumulation of the tracer on the left side of the tundish, and a smaller difference in tracer concentration between the two sides of the tundish.

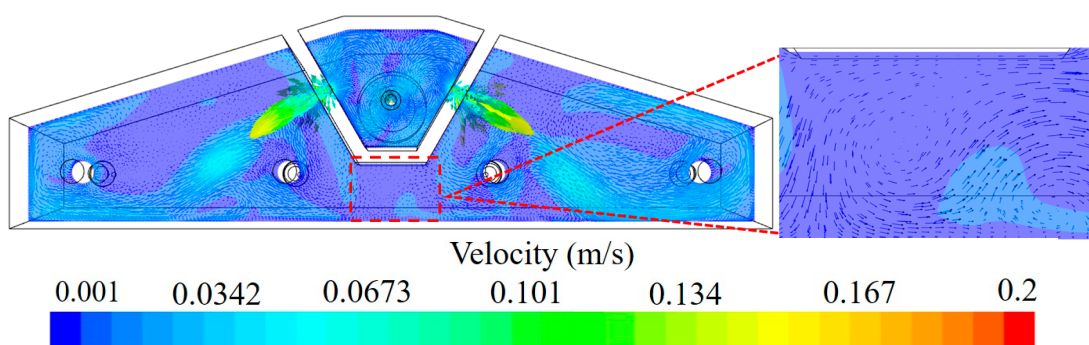


Figure 24. Velocity vector distribution of U-shaped weir tundish after strand 2 sudden blockage at 1200 s.

3.5. Transport Process of the Tracer under Different Blocking Conditions in the Tundish with a U-Shaped Weir Structure with Holes in the Front

Figure 25 depicts the velocity vector diagram shortly after sudden blockage and stable blockage of strand 1 in the tundish with a U-shaped weir with holes at the front. The red dashed boxes in Figure 25b is the area on the front wall of the tundish. From the perspective of sudden blockage, due to the existence of the front guide holes, the streams flowing from the front side of the U-shaped weir spread symmetrically to both sides, adjusting the flow field in the tundish's mainstream area. There is no significant change in the mainstream

area of the blocked region and, at this time, the velocity distribution on both sides of the tundish is relatively symmetrical. From the perspective of stable blockage, as the tundish becomes an asymmetric three-strand flow, there is a significant difference in the velocity field distribution between the left and right sides, and the effect of the flow streams from the front side of the U-shaped weir on the unblocked side is noticeably weakened. Figure 26 shows the velocity vector results of the tundish at 1200 s after sudden blockage of strand 1. From the figure, it can be observed that after sufficient development, the velocity field is essentially consistent with the stable blockage scheme. The front guide holes continue to affect the flow in the blocked side, while this effect on the unblocked side is diminished.

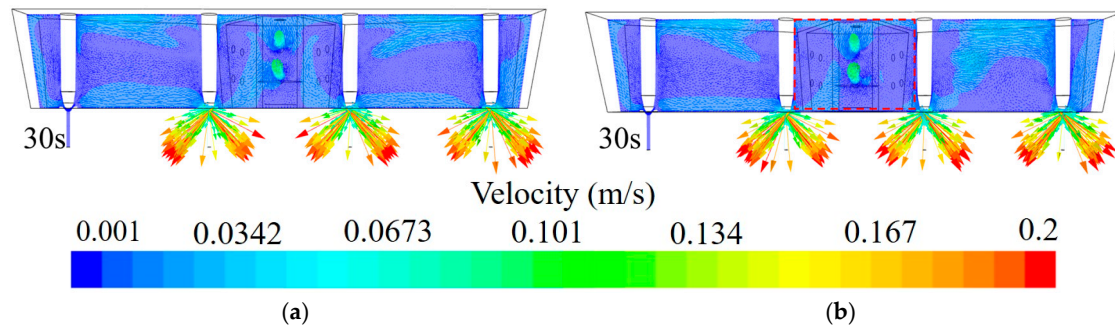


Figure 25. Velocity vector diagram of the tundish with a U-shaped weir with holes in the front after strand 1 blockage at 30 s: (a) sudden blockage; (b) stable blockage.

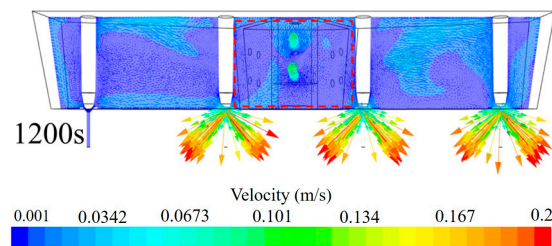


Figure 26. Velocity vector diagram of the tundish at 1200 s with a U-shaped weir with holes in the front under strand 1 sudden blockage.

In Figure 27, the streamline variations under single-strand blockage in the U-shaped weir structure with holes in the front are depicted. When strand 1 is blocked, under both sudden and stable blockage conditions, the transport process of the tracer within the tundish remains essentially consistent. That is, after homogenization in the pouring chamber, a large amount of the tracer flows from the left, right, and front guide holes to the mainstream area. The tracer flowing out from the left and right sides reaches above stopper rods 1 and 4 along the free surface, where the majority of the tracer forms a counterclockwise circulation flow field (from a frontal perspective), while a small portion forms a clockwise circulation along the edge of the free surface (from a top-down perspective).

Figures 28 and 29 show the velocity vector distributions of the tundish constructed with a U-shaped weir with holes in the front at 1200 s after sudden blockage of strand 1 and strand 2, respectively. The streams flowed out from the front guide holes and spread toward both sides of the tundish. Figure 30 illustrates the schematic diagram of the flow field in the tundish under single-strand blockage. The presence of the front guide holes promotes mixing of the tracer in the mainstream areas on both sides. After 150 s, the flow field in the sudden blockage scenario gradually stabilizes, forming a stable three-stream flow field. Compared to both the double-weir structure and the U-shaped weir structure, the transition time from the flow field in the U-shaped weir structure with holes in the front to a stable state is reduced by 50 s. By 230 s, the tracer concentration in the mainstream areas on both sides remains essentially consistent, and both the stable blockage and sudden blockage scenarios exhibit consistency. Therefore, compared to the two other types of weir

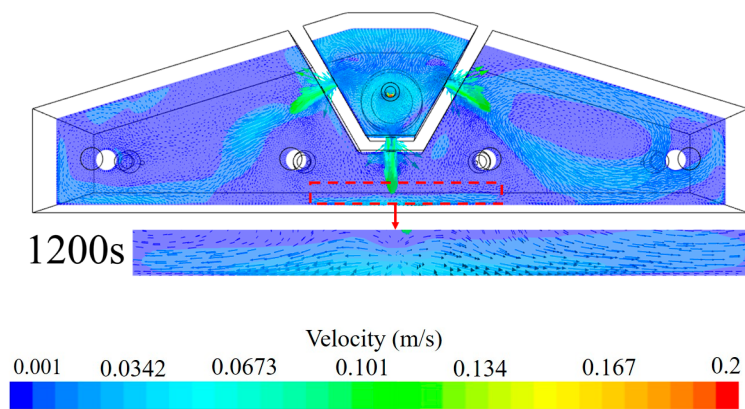


Figure 28. Velocity vector distribution of U-shaped weir tundish with holes in the front when strand 1 is suddenly blocked at 1200 s.

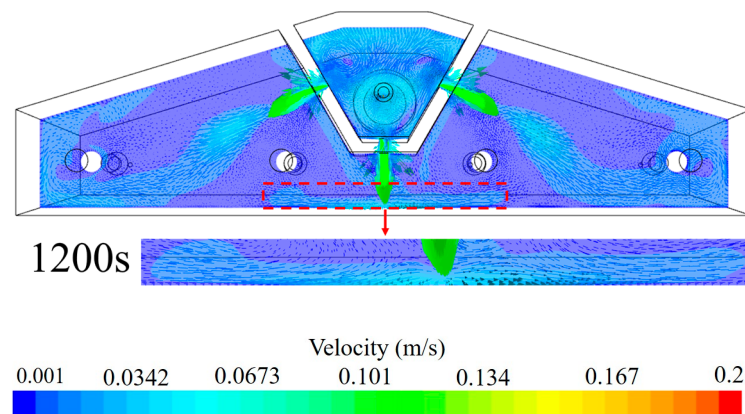


Figure 29. Velocity vector distribution of U-shaped weir tundish with holes in the front when strand 2 is suddenly blocked at 1200 s.

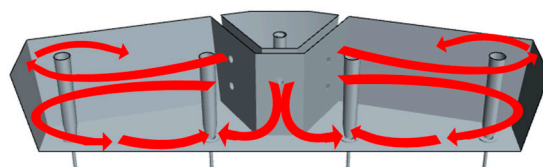


Figure 30. Flow field diagram of the U-shaped weir structure with holes in the front under strand 1 blockage.

3.6. Analysis of RTD for the Stable and Sudden Blockage Conditions

Figures 31 and 32 present the RTD curves under stable and sudden blockage conditions for each strand of the double-weir tundish. After blockage of strand 1 of the double-weir tundish, compared with the minimum response time of blocked strand 2, it is evident that the sudden blockage condition is significantly shorter than the stable blockage condition.

The minimum response time of unblocked strands 3 and 4 remains essentially consistent between the two scenarios. Observing the streamline diagrams at 73 s (Figure 13), it is noted that, in the sudden blockage scenario, a large amount of the tracer moves counterclockwise downward from the right side of stopper rod 1 (in the middle of the tundish) to reach the bottom of the tundish and then moves toward strand 2. Whereas in the stable blockage scenario, a large amount of the tracer follows the stable counterclockwise flow field, passing through the left side of stopper rod 1, descending along the inclined wall surface to reach the bottom of the tundish, and then moves toward strand 2. Hence, it is evident that the tracer's path under the stable blockage condition is longer, resulting

in a prolonged minimum response time, which enhances the retention time of inclusions, facilitating their upward removal.

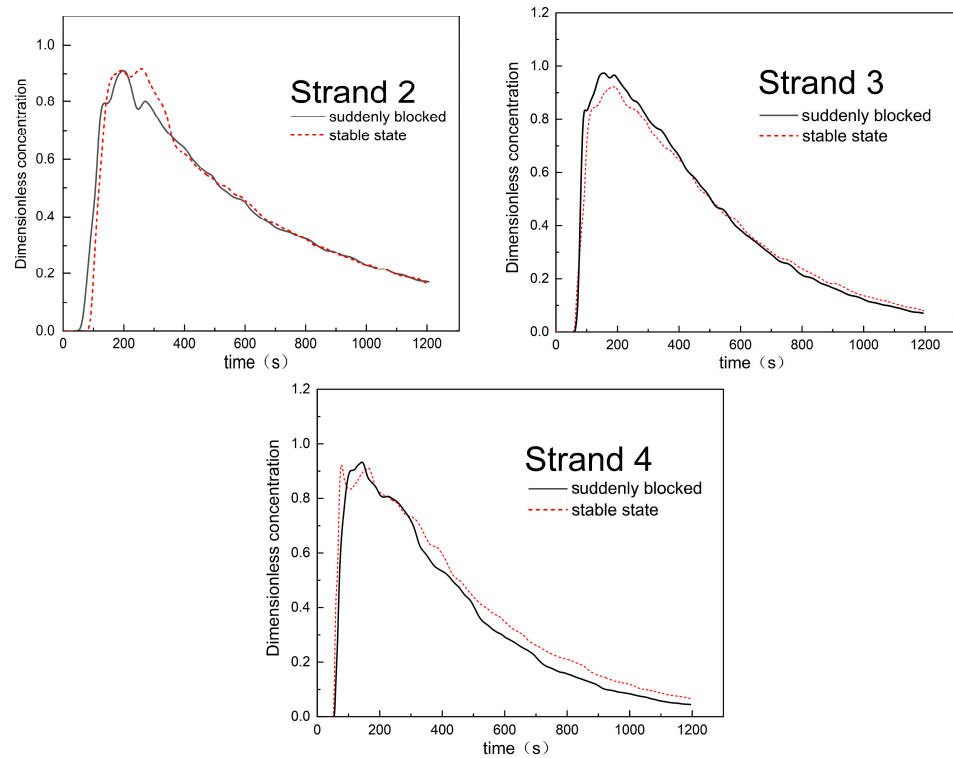


Figure 31. RTD curves of each strand under stable and sudden blockage conditions for strand 1 of the double-weir tundish.

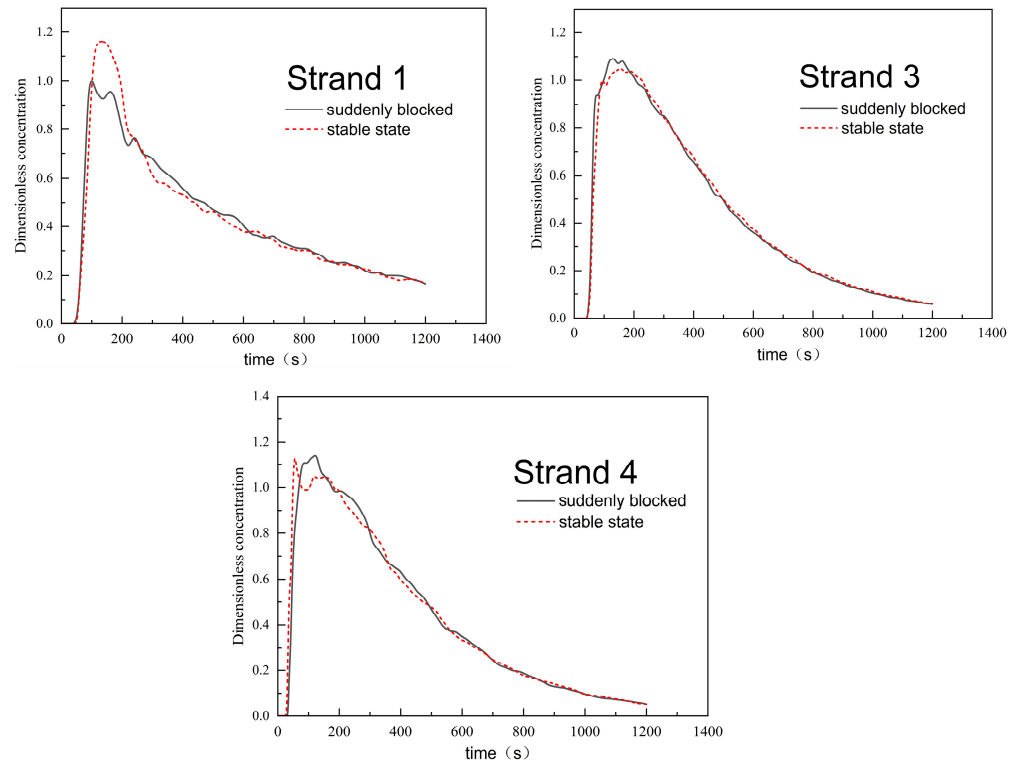


Figure 32. RTD curves of each strand under stable and sudden blockage conditions for strand 2 of the double-weir tundish.

After blockage of strand 2 of the double-weir tundish, we compared the dimensionless peak concentration of the tracer on the blocked side of strand 1. It is evident that, under the stable blockage condition, the dimensionless peak concentration is significantly higher than that under the sudden blockage condition. The peak time under the stable blockage condition is delayed compared to that under the sudden blockage condition, and the RTD curve under the sudden blockage condition exhibits a three-peak phenomenon. Combining the streamline diagram at 73 s (Figure 17) and the flow field schematic diagram (Figure 18), it is analyzed that, under the sudden blockage condition, some of the tracer flows directly toward strand 1, resulting in an earlier peak time. Meanwhile, most of the tracer moves along the bottom toward strand 2, forming a recirculation in the middle of the tundish; hence, multiple peaks appear during the descending phase of the curve. Under the stable blockage condition, the tracer descends along the side wall to reach the bottom of the tundish and is predominantly discharged through strand 1. This results in a higher dimensionless peak concentration.

From the overall RTD curves, at 1200 s, the dimensionless concentration of the tracer at each strand is observed. The dimensionless concentration of the tracer on the blocked side of the strand is significantly higher than that on the unblocked side for strands 3 and 4. Under both scenarios, there is a notable difference in the RTD curves of the unblocked strands on the blocked side. The RTD curves of strands 3 and 4 on the unblocked side are essentially consistent. This indicated that, in the double-weir tundish after single-strand blockage, due to the relative closure of the left and right sides, there exists a certain difference between each strand.

Figures 33 and 34 present the RTD curves of each strand in the stable and sudden blockage scenarios of the U-shaped weir tundish. After single-strand blockage in the U-shaped weir tundish, comparing the RTD curves of the unblocked strands on the blocked side, it is observed that the peak concentration time in the stable blockage scenario precedes that in the sudden blockage scenario. This is attributed to the stable counterclockwise circulation formed inside the tundish in the stable blockage scenario, which is more conducive to the diffusion and outflow of the tracer. After 200 s, the RTD curves under both scenarios largely overlap, indicating that the differences exist within the first 200 s. Specifically, the flow field inside the tundish in the sudden blockage scenario evolves into the initial flow field of the stable blockage scenario after a certain period. Comparing the RTD curves of the unblocked strands, it is evident that the stable blockage scenario exhibits a higher peak concentration and narrower half-peak width, whereas the sudden blockage condition shows a lower peak concentration and wider half-peak width. Combining the streamline diagrams in Figure 21a (85 s) and b (82 s), it can be observed that, at this time, the tracer in the front part of the U-shaped weir spread from the left side to the right side. In the sudden blockage scenario, due to the constantly changing flow field, the movement trajectory of the tracer in the front part of the U-shaped weir becomes chaotic, and the tracer cannot quickly enter the right side but is slowly and continuously replenished to the right side, resulting in an RTD curve resembling a “short and fat bell shape.” In the stable blockage scenario, the flow field is concentrated into a single stream, and the tracer directly enters the right side along the front part of the U-shaped weir from the left side, leading to a steep peak in the RTD curve. Overall, since the left side of the U-shaped weir tundish can supplement the right side, the dimensionless concentration of the remaining tracer inside the tundish is roughly consistent on both sides at 1200 s, but it has a particularly adverse effect on the peak dimensionless concentration of the tracer, especially at strand 3 on the right side.

As shown in Figures 35 and 36, the RTD curves of each flow in the stable and sudden blockage scenarios of the U-shaped weir structure with holes in the front are depicted. After blockage of strand 1, under the stable blockage scenario, the trend of the RTD curve of strand 2 during the first 100 s changes more significantly than that under the sudden blockage scenario. Moreover, the minimum response time and peak concentration are noticeably earlier than those under the sudden blockage scenario. However, after reaching the peak, the curves of both scenarios are essentially the same. Compared to the RTD

curves after single-strand blockage in the double-weir and U-shaped weir tundishes, the differences in the stable and sudden blockage scenarios are smaller. When strand 2 is blocked, the RTD curve of strand 1 under both scenarios only shows a slightly higher peak concentration in the sudden blockage scenario than that in the stable blockage scenario, indicating that the RTD curves are basically consistent for the two schemes of blocking strand 2 in the U-shaped weir structure with holes in the front. Overall, after single-strand blockage, the differences in the RTD curves of strands 3 and 4 on the unblocked side are significantly reduced compared to those in the U-shaped weir tundish. Combining the streamline diagram in Figure 27 (76 s) and Figure 30, it is analyzed that, after passing through the front guide holes, the tracer is distributed to the left and right sides, weakening the diffusion behavior of the tracer from the blocked side to the unblocked side in the U-shaped weir tundish, and thus reducing the significant differences in the RTD curves near strand 3 of the U-shaped weir tundish under both scenarios. This indicated that the presence of front guide holes in the U-shaped weir tundish allows for a more reasonable interconnection of tracers between both sides, which helps to improve the adaptability of both sides of the strand when facing blockage issues.

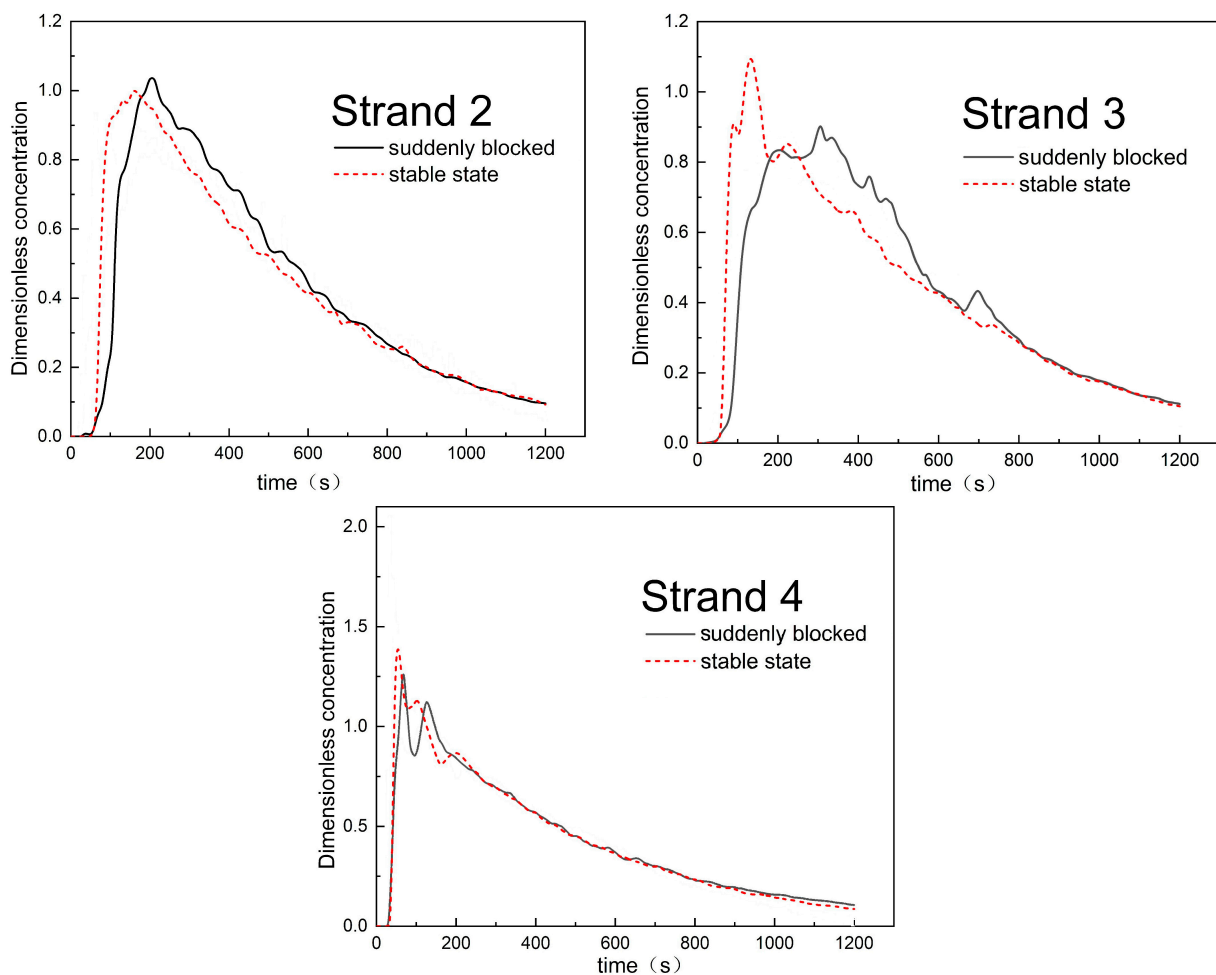


Figure 33. RTD curves of each strand under stable and sudden blockage conditions for strand 1 of the U-shaped weir tundish.

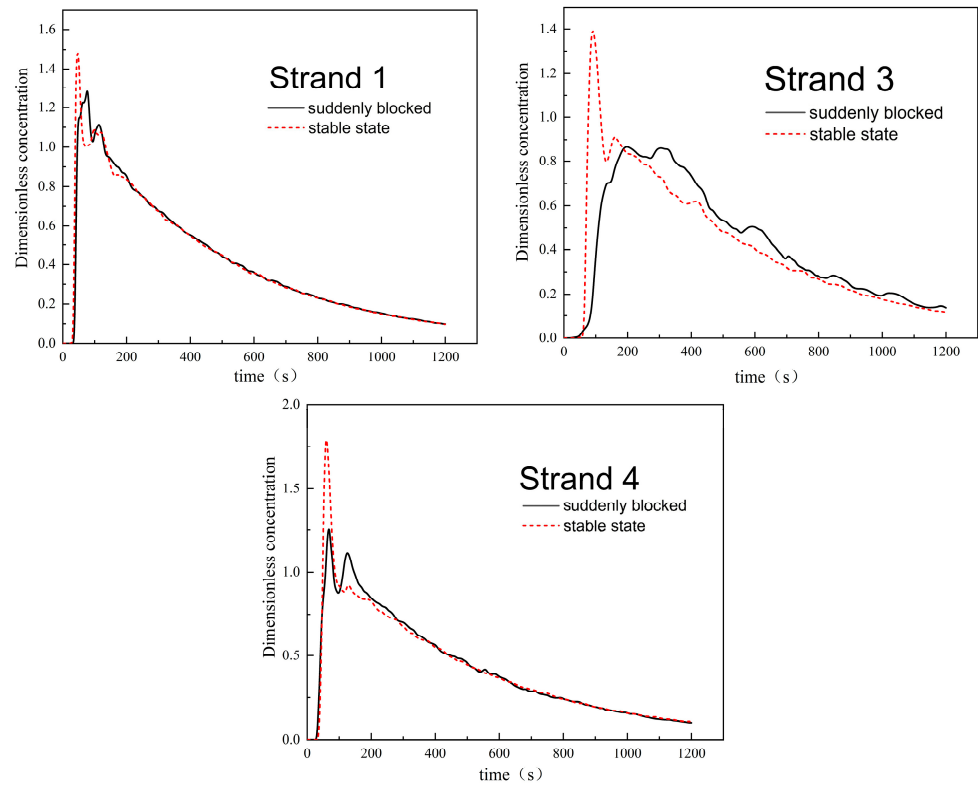


Figure 34. RTD curves of each strand under stable and sudden blockage conditions for strand 2 of the U-shaped weir tundish.

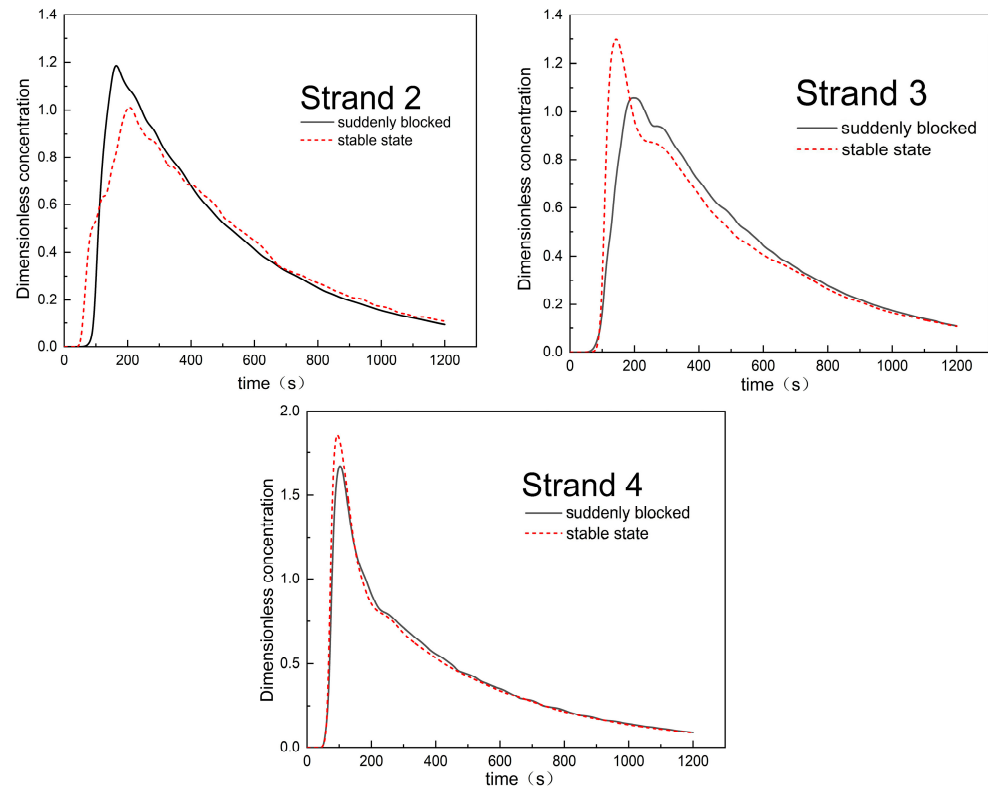


Figure 35. RTD curves of each strand under stable and sudden blockage conditions for strand 1 of the U-shaped weir structure with holes in the front.

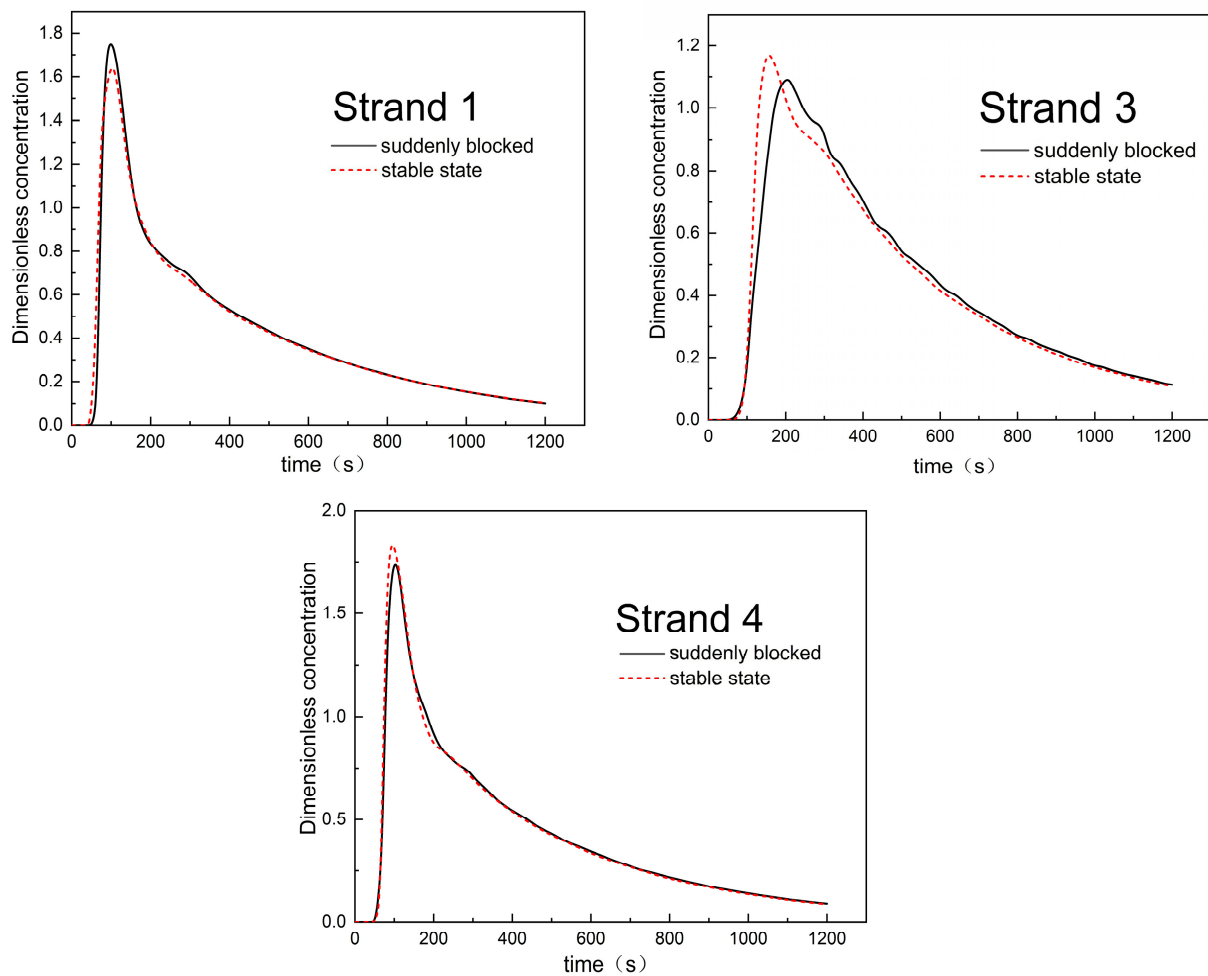


Figure 36. RTD curves of each strand under stable and sudden blockage conditions for strand 2 of the U-shaped weir structure with holes in the front.

3.7. Consistency Analysis of Each Strand with Stable Blockage and Sudden Blockage

The outflow percentage curve charts for stable and sudden blockages in the tundishes with a double weir, U-shaped weir, and U-shaped weir structure with holes in the front are shown in Figures 37–39. It can be observed from the figures that the growth trends of outflow percentage are minimally affected by stable and sudden blockages. According to the flow field, the flow fields of sudden blockage remain consistent with those under the stable blockage condition after 200 s. Therefore, under both blockage conditions, the growth trends of outflow percentage are basically the same. After single-strand blockage in the tundish with a double weir, the outflow percentage of the unblocked strand side decreases significantly, with a greater decrease observed under the sudden blockage condition. This is because the stable counterclockwise circulation flow field has already formed initially under the stable blockage condition, facilitating the stable outflow of the tracer. Whether it is blockage of strand 1 or strand 2, the outflow percentage of strands 3 and 4 remains basically consistent, and it is less affected by stable sudden blockage. This is because the main flow areas on both sides of the tundish with a double weir are relatively independent; thus, blockage on the left side has a smaller impact on the right side. However, due to the relative independence of both sides, compared to the U-shaped weir, the tracer on both sides cannot be mixed uniformly; hence, the consistency of each flow is significantly affected.

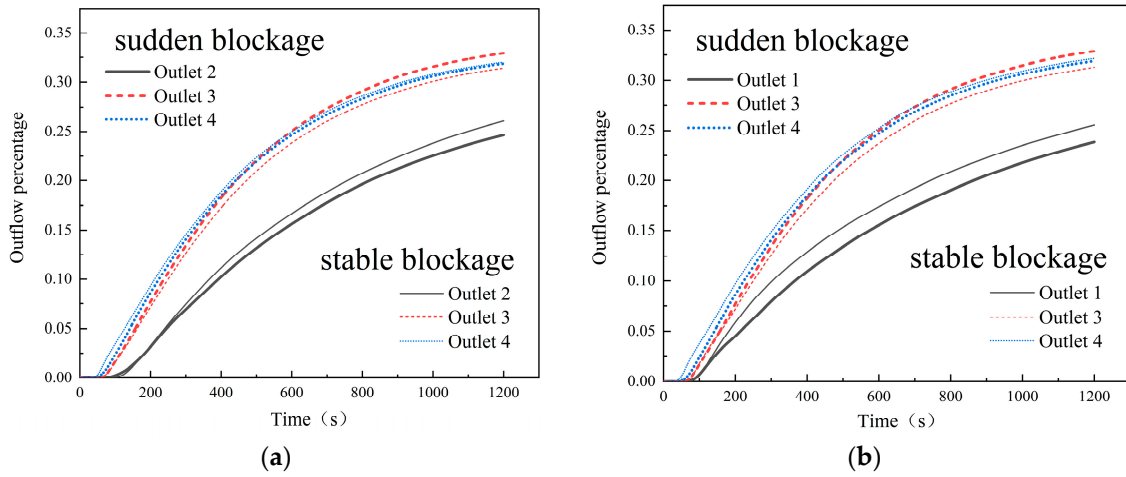


Figure 37. Outflow percentage curve of the double-weir tundish: (a) strand 1 blocked, (b) strand 2 blocked.

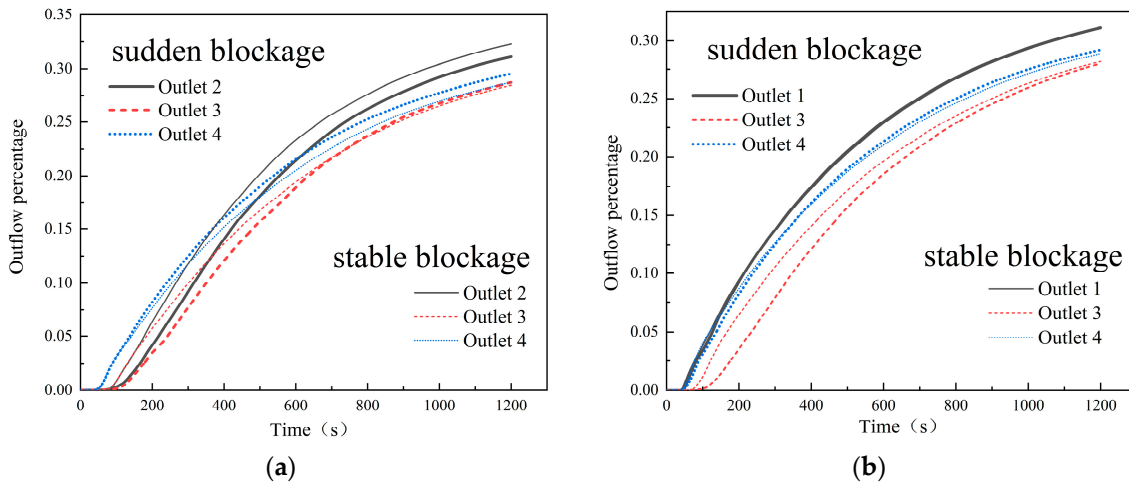


Figure 38. Outflow percentage curve of the U-shaped weir tundish: (a) strand 1 blocked, (b) strand 2 blocked.

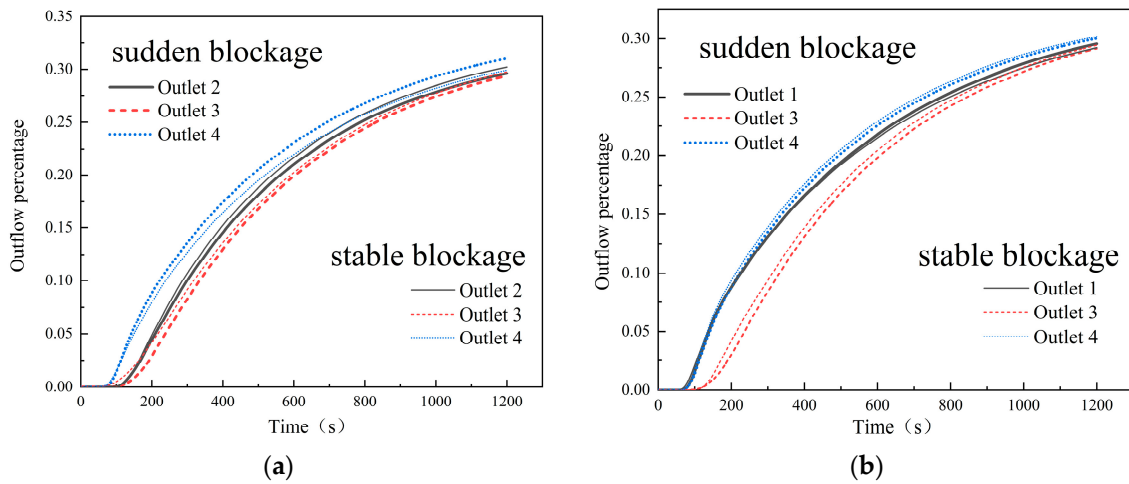


Figure 39. Outflow percentage curve of the U-shaped weir structure with holes in the front: (a) strand 1 blocked, (b) strand 2 blocked.

After single-strand blockage in the tundishes with a U-shaped weir and U-shaped weir structure with holes in the front, due to the interconnection between the left and right sides, the tracer can be better mixed inside the tundish; therefore, the outflow percentage of each strand is not significantly different. The outflow percentage of strand 2 in the tundish with a U-shaped weir is significantly increased, with a greater increase observed under the stable blockage condition. While under stable and sudden blockage conditions in the tundish with a U-shaped weir structure with holes in the front, the outflow percentage of each strand is basically consistent. This is because the diversion holes in the front facilitates mixing of the tracer on both sides, weakening the impact of single-flow blockage and allowing the tundish to quickly form a stable flow field, thus exhibiting better adaptability under different blockage conditions.

Table 3 presents the time-weighted average variance under sudden and stable blockages in the tundishes with a double weir, U-shaped weir, and U-shaped weir structure with holes in the front. It can be observed from the table that, except for blockage of strand 1 in the tundish with a U-shaped weir, the average variance under the stable blockage scheme is smaller than that under the sudden blockage scheme. This is because under the stable blockage scheme, the flow field is more stable, facilitating uniform mixing of tracer. The average variance of the tundish with a U-shaped weir is significantly lower than that of the tundish with a double weir, once again proving that interconnection between the main flow areas on both sides can effectively weaken the impact of single-strand blockage. As shown in Figure 40, under the stable blockage condition, the consistency of each flow is optimal in the tundish with a U-shaped weir structure with holes in the front among all schemes.

Table 3. Time-weighted variance of the double-weir tundish, U-shaped weir tundish, and U-shaped weir structure with holes in the front under single-strand sudden blockage or stable blockage.

Time-Weighted Variance	Double-Weir Tundish		U-Shaped Weir Tundish		U-Shaped Weir Structure with Holes in the Front	
	Sudden Blockage	Stable Blockage	Sudden Blockage	Stable Blockage	Sudden Blockage	Stable Blockage
strand 1 blocked	2.02×10^{-3}	1.42×10^{-3}	2.76×10^{-4}	3.09×10^{-4}	3.01×10^{-4}	1.16×10^{-4}
strand 2 blocked	2.09×10^{-3}	1.22×10^{-3}	4.88×10^{-4}	2.59×10^{-4}	2.84×10^{-4}	2.26×10^{-4}

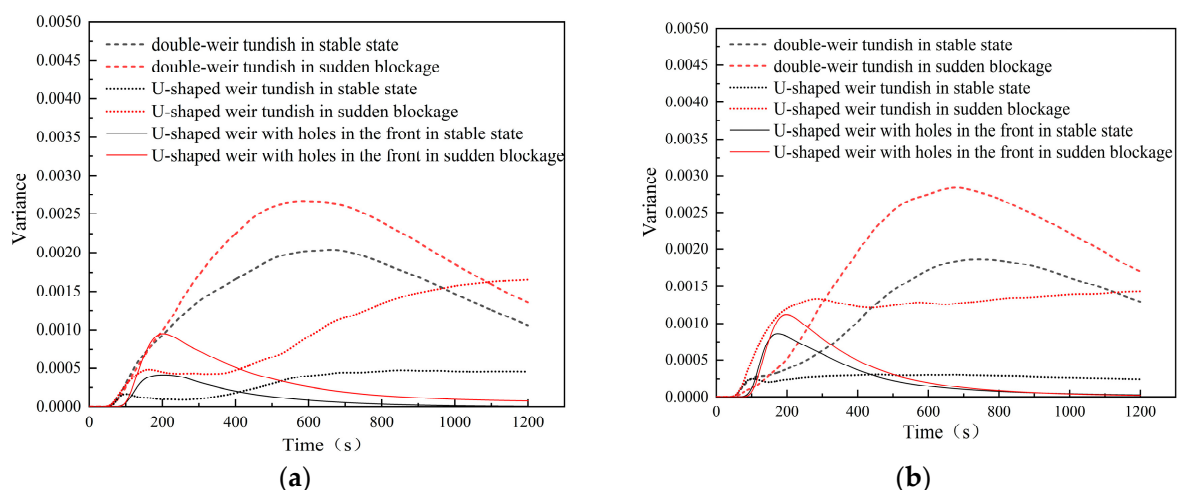


Figure 40. Variance curve of each scheme: (a) strand 1 blocked, (b) strand 2 blocked.

3.8. Discussion

In this paper, the flow characteristics after stable and sudden blockages of tundish outlets under abnormal conditions were compared. The novelty and the contribution of the present work when compared with reference [37] are clarifying the difference between sudden blockage during the operation of tundish casting and the fewer strand operation

used by the four-strand tundish as the three-strand tundish. Furthermore, in this paper, we compare the flow fields, velocity fields, RTD curves, and outflow percentage curves of the tundishes with three different weir structures under sudden blockage and stable blockage conditions. In the case of sudden blockage of the tundish strand, the new design of a U-shaped weir structure with holes in the front can adjust the flow field compared to the other two structures. It can mitigate the effects of strand sudden blockage and achieve better consistency among strands.

In the tundish with a double weir, due to the independent flow fields on both sides, a concentration difference occurs on both sides of the tundish after single-strand blockage, with a greater concentration difference observed in the sudden blockage scheme compared to the stable blockage scheme, resulting in poorer consistency among strands. In the tundishes with a U-shaped weir and U-shaped weir structure with holes in the front, the structure allowing communication between the left and right pouring areas exhibited better adaptability after single-flow blockage, effectively reducing differences on both sides and improving the consistency among strands. At the same time, it is noted that the erosion of refractory materials by molten steel will reduce the service life of the tundish [50,51], as the spalling of refractory materials can lead to the generation of large-sized inclusions in the steel. When the U-shaped weir has guide holes in the front side, the molten steel will erode the front wall of the tundish to a certain extent, increasing the degree of erosion of the refractory materials. Q. Wang et al. [52] conducted a study on the erosion rate of refractory materials in various parts of the tundish using physical and mathematical models. The results indicated that the refractory materials inside the turbulence inhibitor experience the most severe erosion, while other areas outside the turbulence inhibitor can be neglected.

Regarding the temperature difference after blockage, L. Zhang et al. [33] found that, in a four-strand tundish, the maximum temperature difference was 29 °C for single-strand blockage and 40 °C for double-strand blockage. The blockage of strands has a certain impact on the temperature field of the tundish. Therefore, in subsequent work, attention may be paid to the temperature variations of the tundish under abnormal conditions, and the influence of different weir structures on the temperature field of the tundish may be analyzed. However, from an industrial partner's feedback, the temperature difference in strands is not a big issue since they can adjust the cooling in molds and secondary cooling in strands to control the macrostructure and quality of small-sized billets and blooms. Anyway, this is our future work on this topic.

Because of the different flow fields formed in the front of the U-shaped weir under stable and sudden blockage schemes, differences occur in the outlets near the U-shaped weir on the right side of the tundish, manifested in the peak values and peak times of the RTD curves. Therefore, by setting diversion holes on the front side of the U-shaped weir, both sides of the tundish received tracer replenishment, effectively reducing differences near the outlets on the front side of the U-shaped weir under both schemes.

This paper only considers one type of structure allowing flow between the left and right sides. The position of the front weir of the tundish, the positions, angles, and numbers of diversion holes, and the design of turbulence inhibitors all affect the degree of mixing in the left and right pouring areas. Based on the results of this paper, it is important to differentiate between sudden and stable blockages when studying tundish closure and conduct calculations and simulations tailored to the specific scenarios to achieve more accurate and realistic results.

4. Conclusions

1. After sudden blockage of the four-strand tundish, its flow field does not immediately transition to a stable three-strand flow field, but rather maintains the four-strand flow field before blockage, gradually approaching a stable three-strand flow field, ultimately remaining basically consistent with the flow field under stable blockage conditions.

2. Under four-strand casting conditions, the velocity vector fields of the three tundish cases remain symmetric on the left and right sides. At 30 s after sudden blockage, only the velocity vector of the U-shaped weir with holes in the front case maintain symmetry on both sides. At 1200 s after sudden blockage, the velocity vectors of all three tundish cases are consistent with those of the stable blockage case.
3. After sudden blockage of the tundish strands, using different structures of weir, the transition of the flow field from an unstable four-strand flow field to a stable three-strand flow field varies in time. The tundish with a double weir and the tundish with a U-shaped weir reach a stable state after 200 s, while the tundish with a U-shaped weir structure with holes in the front reaches stability after 150 s.
4. The flow field under stable blockage conditions is more stable compared to that under sudden blockage, and the consistency among strands is higher than under sudden blockage.
5. After single-strand blockage, the influence on the unblocked outlets on the same side is significant, especially for the tundish with a double weir, where the weir separates the left and right sides into independent parts, resulting in minimal impact on the flow field on the right side if blockage occurs on the left side.
6. In both stable and sudden blockage scenarios, the outflow percentage curves and flow fields of the tundish with a U-shaped weir with structure holes in the front remain basically consistent, indicating that, after sudden blockage, the influence of blockage on each strand is minimal, demonstrating better adaptability.
7. Under single-strand blockage, the consistency among strands of the tundish with a U-shaped weir structure with holes in the front is optimal, effectively adjusting the flow pattern from the blocked side to the unblocked side.

Author Contributions: Conceptualization, C.C., J.F., Z.G. and Y.L. (Yanzhao Luo); methodology, C.C., J.S. and J.F.; software, J.S., T.W. and M.G.; validation, Y.L. (Yuqian Li), J.S. and T.W.; formal analysis, J.S. and Y.L. (Yuqian Li); investigation, J.S., M.G., Y.L. (Yanzhao Luo) and C.C.; resources, J.F., C.C., Y.L. (Yanzhao Luo) and Z.G.; data curation, J.S., M.G., T.W. and Y.L. (Yuqian Li); writing—original draft preparation, J.S. and Y.L. (Yuqian Li); writing—review and editing, J.F., Z.G., C.C. and Y.L. (Yanzhao Luo); visualization, J.S., W.L. and Y.L. (Yuqian Li); supervision, J.F., W.L., C.C. and Y.L. (Yanzhao Luo); project administration, C.C. and J.F.; funding acquisition, C.C. All authors have read and agreed to the published version of the manuscript.

Funding: This research was funded by the Applied Fundamental Research Programs of Shanxi Province, grant number 202303021221036; Research Project Supported by Shanxi Scholarship Council of China, grant number 2022-040; and “Chunhui Plan” Collaborative Research Project by the Ministry of Education of China, grant number HZKY20220507.

Data Availability Statement: The original contributions presented in the study are included in the article, further inquiries can be directed to the corresponding authors.

Acknowledgments: Ruihua Qin is acknowledged for discussions on industrial control of continuous casting under fewer strand operation.

Conflicts of Interest: Author Y.L. was employed by the company Beijing Research Institute of Technology of Shougang Group Co., Ltd. The remaining authors declare that the research was conducted in the absence of any commercial or financial relationships that could be construed as a potential conflicts of interest.

References

1. Mazumdar, D.; Guthrie, R.I.L. The Physical and Mathematical Modelling of Continuous Casting Tundish Systems. *ISIJ Int.* **1999**, *39*, 524–547. [[CrossRef](#)]
2. Walek, J.; Tkadlečková, M.; Velička, M.; Machů, M.; Cupek, J.; Huczala, T.; Cibulka, J.; Růžička, J.; Michalek, K. Physical Experiments and Numerical Simulations of the Influence of Turbulence Inhibitors and the Position of Ladle Shroud on the Steel Flow in an Asymmetric Five-Strand Tundish. *Metals* **2023**, *13*, 1821. [[CrossRef](#)]
3. Chang, S.; Song, H.; Liu, Z.; Zou, Z.; Shao, L.; Li, B. Experimental Study on Bubble Entrainment by a Free Fall Jet in an Argon-Filled Continuous Casting Tundish. *Steel Res. Int.* **2023**, *94*, 2200287. [[CrossRef](#)]

4. Lin, P.; Jin, Y.; Gan, F.; Ma, G.; Cheng, C.; Li, Y.; Liu, Z.; Li, J.; Huang, J. Study of the Impact of Opening Streams on Turbulence Inhibitors in Tundishes. *Met. Mater. Trans. B* **2022**, *53*, 3159–3169. [[CrossRef](#)]
5. Zhang, J.; Qin, B.; Liu, Y.; Li, Q.; Zuo, X.; Wang, C.; Yang, S.; Liu, Q. Multiphase flow inside a four-strand continuous casting tundish using three types of ladle shrouds. *J. Iron Steel Res. Int.* **2023**, *30*, 1171–1181. [[CrossRef](#)]
6. Chen, C.; Ni, P.Y.; Jonsson, L.T.I.; Tilliander, A.; Cheng, G.G.; Jönsson, P.G. A Model Study of Inclusions Deposition, Macroscopic Transport, and Dynamic Removal at Steel–Slag Interface for Different Tundish Designs. *Met. Mater. Trans. B* **2016**, *47*, 1916–1932. [[CrossRef](#)]
7. Tkadlečková, M.; Walek, J.; Michalek, K.; Huczala, T. Numerical Analysis of RTD Curves and Inclusions Removal in a Multi-Strand Asymmetric Tundish with Different Configuration of Impact Pad. *Metals* **2020**, *10*, 849. [[CrossRef](#)]
8. Chang, S.; Zou, Z.; Li, B.; Isac, M.; Guthrie, R.I.L. Modeling Inclusion Removal when Using Micro-bubble Swarm in a Full-Scale Tundish with an Impact Pad. *Met. Mater. Trans. B* **2022**, *53*, 526–536. [[CrossRef](#)]
9. Xie, Q.; Ni, P.; Ersson, M.; Jonsson, P.; Li, Y. Numerical Simulations on Dynamic Behavior of Multiphase Flow and Heat Transfer in a Round Mold with a Swirling Flow Tundish Design. *Met. Mater. Trans. B* **2022**, *53*, 3197–3214. [[CrossRef](#)]
10. Chen, H.; Liu, Z.; Li, F.; Lyu, B.; Chen, W.; Zhang, L. Numerical Simulation on Multiphase Flow and Slag Entrainment During Casting Start of a Slab Continuous Casting Tundish. *Met. Mater. Trans. B* **2023**, *54*, 2048–2065. [[CrossRef](#)]
11. Guarneros, J.; Morales, R.D.; Gutierrez, E. Optimized Fluid Flow Control System for a Tundish Used in Frequent Steel Grade Change Operations. *Steel Res. Int.* **2023**, *94*, 2200809. [[CrossRef](#)]
12. Tie, Z.; Tang, H.; Wang, K.; Miao, H.; Cai, S.; Xian, F.; Zhang, J. Effect of Flow Field Optimization of an Asymmetric Multi-Strand Tundish on the Quality Consistency of Cracking Con-Rod Steel. *Materials* **2022**, *15*, 3698. [[CrossRef](#)] [[PubMed](#)]
13. Wu, D.; Liu, J.; Wu, D.; Zhou, P. Evaluation of Molten Steel Flow Behaviors in a Multistrand Tundish via Numerical Simulation and Grey Relational Analysis with a New Dimensionless Operator. *Steel Res. Int.* **2023**, *95*, 2300336. [[CrossRef](#)]
14. Liu, Z.; Li, Y.; Cheng, C.; Lan, P.; Wu, W. Study on Parameter Optimization of Diversion Wall in an Eight-Strand Tundish during Continuous Casting of Billet with High Casting Speed. *Processes* **2022**, *10*, 555. [[CrossRef](#)]
15. Zhu, H.; Wang, M.; Yao, C.; Wang, Z.; Wang, X.; Bao, Y. Influence of non-iso-velocity casting on flow-field index of a 41-ton six-strand tundish by physical and numerical modeling. *J. Iron Steel Res. Int.* **2023**, *30*, 51–63. [[CrossRef](#)]
16. Mukherjee, S.; Mazumdar, D. Physical and Mathematical Modeling of Argon Flow and Distribution Around a Ladle Shroud-Collector Nozzle (LS-CN) Assembly. *Met. Mater. Trans. B* **2022**, *53*, 2600–2617. [[CrossRef](#)]
17. Xin, Z.; Cui, H.; Li, T.; Tang, G.; Zhu, Y.; Yan, J.; Li, J. Numerical Simulation of Inclusion Removal by Bubble Injection in the Submerged Nozzle with Swirling Flow. *Met. Mater. Trans. B* **2022**, *53*, 2570–2586. [[CrossRef](#)]
18. Yang, B.; Deng, A.; Duan, P.; Kang, X.; Wang, E. “Power curve” key factor affecting metallurgical effects of an induction heating tundish. *J. Iron Steel Res. Int.* **2022**, *29*, 151–164. [[CrossRef](#)]
19. Zhang, Q.; Xu, G.; Iwai, K. Optimization of the Circular Channel Size and the A.C. Magnetic Field Parameters for Application in a Channel-Type Induction-Heating Tundish. *Metals* **2024**, *14*, 420. [[CrossRef](#)]
20. Quan, Q.; Zhang, Z.; Qu, T.; Li, X.; Tian, J.; Wang, Y. Physical and numerical investigation on fluid flow and inclusion removal behavior in a single-strand tundish. *J. Iron Steel Res. Int.* **2023**, *30*, 1182–1198. [[CrossRef](#)]
21. Li, Q.; Qin, B.; Zhang, J.; Dong, H.; Li, M.; Tao, B.; Mao, X.; Liu, Q. Design Improvement of Four-Strand Continuous-Casting Tundish Using Physical and Numerical Simulation. *Materials* **2023**, *16*, 849. [[CrossRef](#)]
22. Cwudziński, A.; Pieprzyca, J.; Merder, T. Numerical and Physical Modeling of Liquid Steel Asymmetric Behavior during Non-Isothermal Conditions in a Two-Strand Slab Tundish—“Butterfly Effect”. *Materials* **2023**, *16*, 6920. [[CrossRef](#)] [[PubMed](#)]
23. Chen, X.; Xiao, H.; Wang, P.; He, H.; Zhang, J. Magnetic-Flow-Thermal Characteristics of An Innovative Four-Channel Induction Heating Tundish. *Steel Res. Int.* **2022**, *93*, 2100839. [[CrossRef](#)]
24. Yao, C.; Wang, M.; Zhu, H.; Xing, L.; Bao, Y. Mathematical Study of Realistic Removal Rates of Non-metallic Inclusions in Continuous Casting Tundish Using Optimized Criterion. *Met. Mater. Trans. B* **2023**, *54*, 1144–1158. [[CrossRef](#)]
25. Liu, C.; Xiao, A.; He, Z.; Yan, W.; Li, G.; Wang, Q. Numerical Investigation on Motion and Removal of Inclusions in Continuous Casting Tundish with Multiorifice Filter. *Steel Res. Int.* **2022**, *93*, 2100818. [[CrossRef](#)]
26. Bruch, C.; Valentin, P. Mathematical Modelling of Fluid Flow in a Continuous Casting Tundish with regard to Extraordinary Casting Conditions. *Steel Res. Int.* **2004**, *75*, 659–665. [[CrossRef](#)]
27. Sengupta, A.; Mishra, P.; Singh, V.; Mishra, S.; Jha, P.K.; Ajmani, S.K.; Sharma, S.C. Physical modelling investigation of influence of strand blockage on RTD characteristics in a multistrand tundish. *Ironmak. Steelmak.* **2013**, *40*, 159–166. [[CrossRef](#)]
28. Merder, T. Numerical Investigation of the Hydrodynamic Conditions in A Multi-Strand Cc Tundish with Closed Outlets. *Arch. Met. Mater.* **2014**, *59*, 891–896. [[CrossRef](#)]
29. Mishra, S.K.; Jha, P.K.; Sharma, S.C.; Ajmani, S.K. Effect of blockage of outlet nozzle on fluid flow and heat transfer in continuously cast multistrand billet caster tundish. *Can. Met. Q.* **2012**, *51*, 170–183. [[CrossRef](#)]
30. Xie, W.; Bao, Y.; Zhang, L.; Wang, M.; Li, R. Research on Small Stream Pouring of Seven Machine Tundish with Seven Streams. *Foundry Technol.* **2014**, *35*, 2070–2072.
31. Zhang, J.; Li, J.; Yang, S. Optimization of Fluid Flow in a Twelve-strand Continuous Casting Tundish with Two Strands Closed. *Metall. Int.* **2014**, *19*, 10.
32. Braun, A.; Warzecha, M.; Pfeifer, H. Numerical and Physical Modeling of Steel Flow in a Two-Strand Tundish for Different Casting Conditions. *Met. Mater. Trans. B* **2010**, *41*, 549–559. [[CrossRef](#)]

33. Zhang, L. Fluid Flow, Heat Transfer and Inclusion Motion in a Four-Strand Billet Continuous Casting Tundish. *Steel Res. Int.* **2005**, *76*, 784–796. [[CrossRef](#)]
34. Huang, X. Numerical Simulation Study on Plug Flow Operation of Tenstrand Tundish. *Contin. Cast.* **2018**, *43*, 35–40. [[CrossRef](#)]
35. Zhong, L.; Wang, M.; Chen, B.; Wang, C.; Zhu, Y. Flow Control in Six-Strand Billet Continuous Casting Tundish with Different Configurations. *J. Iron Steel Res. Int.* **2010**, *17*, 7–12. [[CrossRef](#)]
36. Yao, C.; Wang, M.; Pan, M.; Bao, Y. Optimization of large capacity six-strand tundish with flow channel for adapting situation of fewer strands casting. *J. Iron Steel Res. Int.* **2021**, *28*, 1114–1124. [[CrossRef](#)]
37. Fan, J.; Li, Y.; Chen, C.; Ouyang, X.; Wang, T.; Lin, W. Effect of Uniform and Non-Uniform Increasing Casting Flow Rate on Dispersion and Outflow Percentage of Tracers in Four Strand Tundishes under Strand Blockage Conditions. *Metals* **2022**, *12*, 1016. [[CrossRef](#)]
38. Wang, X.; Wang, S.; Hu, H.; Xie, X.; Wu, C.; Chen, D.; Long, M. Flow Behavior of Liquid Steel in Fewer Strands Casting of Six-Strand Bloom Tundish. *Metals* **2023**, *13*, 706. [[CrossRef](#)]
39. Chen, C.; Cheng, G.G.; Yang, H.K.; Hou, Z.B. Physical Modeling of Fluid Flow Characteristics in a Delta Shaped, Four-Strand Continuous Casting Tundish with Different Flow Control Devices. *Adv. Mater. Res.* **2011**, *284*, 1071–1079. [[CrossRef](#)]
40. Assael, M.J.; Kakosimos, K.; Banish, R.M.; Brillo, J.; Egry, I.; Brooks, R.; Quested, P.N.; Mills, K.C.; Nagashima, A.; Sato, Y.; et al. Reference Data for the Density and Viscosity of Liquid Aluminum and Liquid Iron. *J. Phys. Chem. Ref. Data* **2006**, *35*, 285–300. [[CrossRef](#)]
41. Jeyakumar, M.; Hamed, M.; Shankar, S. Rheology of liquid metals and alloys. *J. Non-Newton. Fluid* **2011**, *166*, 831–838. [[CrossRef](#)]
42. Birs, I.; Muresan, C.; Copot, D.; Ionescu, C. Model Identification and Control of Electromagnetic Actuation in Continuous Casting Process with Improved Quality. *IEEE/CAA J. Autom. Sin.* **2023**, *10*, 203–215. [[CrossRef](#)]
43. Shih, T.-H.; Liou, W.W.; Shabbir, A.; Yang, Z.; Zhu, J. A new $k-\epsilon$ eddy viscosity model for high reynolds number turbulent flows. *Comput. Fluids* **1995**, *24*, 227–238. [[CrossRef](#)]
44. Rodi, W. Experience with two-layer models combining the k -epsilon model with a one-equation model near the wall. In Proceedings of the 29th Aerospace Sciences Meeting, Reno, NV, USA, 7–10 January 1991; ARC: Columbus, OH, USA, 1991; p. 216. [[CrossRef](#)]
45. Patankar, S.V. *Numerical Heat Transfer and Fluid Flow*; Hemisphere Publishing Corporation: New York, NY, USA, 1980.
46. Wolfshtein, M. The velocity and temperature distribution in one-dimensional flow with turbulence augmentation and pressure gradient. *Int. J. Heat Mass Transf.* **1969**, *12*, 301–318. [[CrossRef](#)]
47. Chen, C.; Jonsson, L.T.I.; Tilliander, A.; Cheng, G.; Jönsson, P.G. A mathematical modeling study of the influence of small amounts of KCl solution tracers on mixing in water and residence time distribution of tracers in a continuous flow reactor-metallurgical tundish. *Chem. Eng. Sci.* **2015**, *137*, 914–937. [[CrossRef](#)]
48. Ouyang, X.; Lin, W.; Luo, Y.; Zhang, Y.; Fan, J.; Chen, C.; Cheng, G. Effect of Salt Tracer Dosages on the Mixing Process in the Water Model of a Single Snorkel Refining Furnace. *Metals* **2022**, *12*, 1948. [[CrossRef](#)]
49. Siemens. *STAR-CCM+ Version 13.04 User Guide*; Siemens PLM Software: Munich, Germany, 2019.
50. Wang, Y.; Yang, J.; Wang, B.; Zhang, H.; Han, J.; Pei, P.; Lv, W.; Zhou, J. Permanent lining castable with low bulk density and thermal conductivity: Bauxite castable for tundish obtained by adding pearlescent sand. *J. Iron Steel Res. Int.* **2024**, *31*, 634–646. [[CrossRef](#)]
51. Yu, C.; Dong, B.; Chen, Y.; Ma, B.; Ding, J.; Deng, C.; Zhu, H.; Di, J. Enhanced oxidation resistance of low-carbon MgO–C refractories with ternary carbides: A review. *J. Iron Steel Res. Int.* **2022**, *29*, 1052–1062. [[CrossRef](#)]
52. Wang, Q.; Tan, C.; Huang, A.; Yan, W.; Gu, H.; He, Z.; Li, G. Quantitative Characterization of Flow-Induced Erosion of Tundish Refractory Lining via Water Model Experiment and Numerical Simulation. *Met. Mater. Trans. B* **2021**, *52*, 3265–3272. [[CrossRef](#)]

Disclaimer/Publisher’s Note: The statements, opinions and data contained in all publications are solely those of the individual author(s) and contributor(s) and not of MDPI and/or the editor(s). MDPI and/or the editor(s) disclaim responsibility for any injury to people or property resulting from any ideas, methods, instructions or products referred to in the content.